

Characterization of autonomous direct methanol fuel cell systems with various designs for portable applications

Von der Fakultät für Maschinenbau
der Technischen Universität Carolo-Wilhelmina zu Braunschweig

zur Erlangung der Würde

eines Doktor-Ingenieurs (Dr.-Ing.)

genehmigte Dissertation

von: M.Sc. Youngseung Na
geb. am 02. Januar 1978 in Seoul, Republik Korea

eingereicht am: 08.12.2016
mündliche Prüfung am: 02.05.2017

Gutachter:

Frau Prof. Dr.-Ing. Ulrike Krewer
Herr Prof. Dr.-Ing. Achim Kienle
Herr Prof. Dr.-Ing. Jürgen Köhler

(Referent/Betreuer)
(Referent)
(Vorsitzender)

2017

Contents

Statement of authorship	7
Kurzfassung	9
Abstract	11
Acknowledgment	13
1 Introduction	15
1.1 Introductory explanation of fuel cells	15
1.2 State of the art	17
1.3 Motivation and scope of this work	19
2 Reference system	21
2.1 Review of modelling [1]	22
2.1.1 Multicomponent equilibrium	22
2.1.2 Fuel cell	23
2.1.3 Coolers	26
2.1.4 Separators	26
2.1.5 Mixer	27
2.1.6 Controllers	28
2.2 Experiment	32
2.2.1 System components	33
2.2.2 Setup for steady state analysis	36
2.2.3 Setup for dynamic behaviour analysis	38
2.2.4 Potential error analysis	40
2.3 Results and discussion	40
2.3.1 Steady state analysis	40
2.3.2 Dynamic behaviour analysis	43

2.4	Conclusions	44
3	System variation for high efficiency	51
3.1	System modifications	52
3.2	Modelling	53
3.2.1	Fuel cell	53
3.2.2	Peripheral devices	54
3.2.3	Controller synthesis	54
3.3	Experimental set-up	62
3.4	Results and discussion	63
3.4.1	Two-mixer system	67
3.4.2	Separate-tank system	67
3.4.3	Faradaic efficiencies	69
3.4.4	Liquid holdup in solution tanks	69
3.5	Conclusions	71
4	System variation for process integration	73
4.1	System modifications	74
4.2	Modelling	75
4.2.1	Fuel cell	76
4.2.2	Cooler	77
4.2.3	Integrated separator	77
4.2.4	Controller synthesis of mingled outlet system	78
4.2.5	Controller synthesis of highly integrated system	82
4.3	Experiment	85
4.3.1	Experimental Setup	85
4.3.2	Operating conditions	85
4.4	Results and discussions	86
4.4.1	Mingled outlet system validation	86
4.4.2	Highly integrated system	90
4.4.3	Efficiency	92
4.5	Conclusions	94
5	Summary and outlook	97
	Nomenclature	101

5.1	Latin symbols	101
5.2	Greek symbols	102
5.3	Superscripts	102
5.4	Subscripts	103
5.5	Diacritics	103
Bibliography		105
List of Tables		111
List of Figures		113

Statement of authorship

Hereby I, M.Sc. Youngseung Na, certify that this doctoral thesis, titled:

"Characterization of autonomous direct methanol fuel cell systems with various designs for portable applications",

was written entirely independently by myself and that it was not used in any other examination before. Furthermore I declare to the best of my knowledge, that no other work with any altered version exists and that all references required for the completion of this work has been marked and cited as such.

Braunschweig, 7th December 2016

Youngseung Na

Kurzfassung

Heutzutage ist die Verwendung tragbarer elektronischer Geräte, wie Laptops, sehr verbreitet. Dort eingesetzte Batterien weisen jedoch immer noch einen sehr niedrigen Energiegehalt auf. Um dies zu kompensieren, wurden seit mehreren Jahrzehnten Brennstoffzellen als Alternative vorgeschlagen. Wegen der Einfachheit des Systemaufbaus eignen sich hauptsächlich Polymer-Elektrolyt-Brennstoffzellen. Obwohl deren Systemaufbau im Vergleich zu anderen Brennstoffzellen einfach ist, sind die Systeme jedoch immer noch groß und schwer.

In der vorliegenden Arbeit wurde als erster Schritt ein *Referenzsystem*, bei dem jede Komponente eine einzelne Funktion erfüllt, anhand von Simulationen im Hinblick auf das stationäre und das dynamische Verhalten untersucht.

Die Modelle für die stationären und dynamischen Analysen konnten anhand von Experimenten bei verschiedenen Umgebungsbedingungen validiert werden. Ein Schwerpunkt lag dabei auch auf autarkem Betrieb, insbesondere hinsichtlich des Betriebs ohne externe Wasser zu- und abfuhr. Die Wasserakkumulationsrate und der dazugehörige autarken Betriebsbereich konnten von erfolgreich in den Simulationsergebnissen reproduziert werden.

In einem weiteren Teil wurden verbesserte Regelalgorithmen entwickelt, um die Faradaysche Effizienz der Systeme zu erhöhen. Auch wurde das Layout des *Referenzsystems* geändert zu einem *Zwei-Mixer-System* mit einem Inline-Mixer, um Konzentrationen schnell anpassen zu können. Ein weiteres, modifiziertes Design, das *separate Tanksystem*, ausgestattet mit separaten Tanks für Wasser und für Methanollösung, wurde entworfen und untersucht. Das *separate Tanksystem* ist in der Lage, die Konzentration des Methanols nicht nur sofort zu erhöhen sondern auch zu verringern. Experimentelle Ergebnisse zeigten, dass das *Zwei-Mixer-System* und das *separate Tanksystem* höhere Faradaysche Wirkungsgrade aufweisen als das *Referenzsystem*.

Schließlich wurden für ein besonders kompaktes System (*vermischte Ausgangssystem*) die Anoden- und Kathodenausgänge zusammengeschal-

tet und über einen gemeinsamen Wärmeübertrager und Gas-Flüssigkeitsseparator geleitet. Um den Verlust an Methanol im Gas-Flüssigkeitsseparator zu verringern, wurde daher ein dynamischer Konzentrationsregler für das *hoch-integrierte System* entwickelt. Dieses *hoch-integrierte System* wurde zusätzlich mit einem integrierten Separator ausgestattet, der die Funktionen eines Mixers und eines Separators verbindet. Dieses System zeigt wegen der dynamischen Konzentrationskontrolle trotz seiner kompakten Größe eine höhere Effizienz als das System ohne integrierten Separator.

Die hier erarbeiteten Simulationen und experimentellen Ergebnisse können als Leitlinien dienen, um zukünftige portable oder auch mobile Brennstoffzellensysteme mit hoher Effizienz oder kompakter Größe zu entwerfen.

Abstract

Most people, who use portable electric devices such as laptops, are experiencing a lack of energy in batteries for portable applications. To compensate or substitute batteries, fuel cells have been suggested for several decades. Among fuel cells, polymer electrolyte fuel cells including direct methanol fuel cells are the most probable type due to the simplicity of systems. Even if the systems are simple compared to other fuel cells, they are still quite heavy and large to carry.

In this work, first of all, the *reference system*, which has each component to carry out a single function, is reviewed for steady state analysis and dynamic behaviour with simulations.

Second, the models for steady state and dynamic analysis are validated with experiments at various environmental conditions. A fuel cell system was installed in a climate chamber, and operated autonomously - without additional water supply. Water accumulation rate and feasibility envelope for autonomous operation are compared with simulation results. Dynamic behaviour of the *reference system* is investigated with dynamic current load as disturbance to controllers such as temperature, concentration or water recovery.

Third, to increase faradaic efficiency of systems, dynamic concentration control algorithms are employed. The layout of the *reference system* is modified to build a *two-mixer system* with an in-line static mixer to adjust concentration quickly. A further modified design, *separate tank system*, which is equipped with separate tanks for water and methanol solution respectively, is examined. The *separate tank system* is able to increase or decrease the methanol concentration immediately. In the experiment, the *two-mixer system* and the *separate tank system* are found out to have higher faradaic efficiency than the *reference system*. However, the additional pump and mixer make the system heavier and bigger than the *reference system*.

Fourth, for a simple and compact system, anode and cathode outlet are integrated into a mingled outlet process to one combined heat exchanger in the system. But it loses a significant amount of gaseous

methanol in a gas-liquid separator after mingled outlet, which decreases fuel efficiency. To reduce methanol loss, a dynamic concentration controller was implemented into the *highly-integrated system*. The *highly-integrated system* is equipped with an integrated separator which combines mixer and separator. In spite of its compact size, the *highly-integrated system* is revealed to have higher efficiency than the *mingled-outlet system* due to dynamic concentration control.

To sum up the five different designs, two highly efficient systems and two integrated systems are investigated systematically with models and validation. These simulation and experimental results can guide to design optimal systems for high efficiency or compact size as portable power sources.

Acknowledgment

At first, I appreciate Prof.Dr.-Ing. Ulrike Krewer for inviting me to Germany. It was my great step to the future and gave a lot of meaningful experiences which would be not possible in my homeland. We discussed a huge amount of scientific issues and different cultures. She became the mentor of my life with sharing her wisdom to live sensibly. She has always encouraged me to accomplish my doctorate in time and properly with warm comments and brilliant advice.

I also especially thank Dr. Federico Zenith, who is working at SINTEF in Norway. He taught me about controlling concept and systematic approach to design experiments. We discussed substantial technologies to accomplish our DFG project. Finally, we succeeded the project, which funded our research of DFG grant KR3850/1-1, "Analysis and design of portable and autonomous direct methanol fuel cell systems."

I also feel thankful to my group members. Dr.-Ing. Maik Kraus kindly guided my first experience in Germany. Dr.-Ing. Daniel Schröder helped me to settle down at Braunschweig and lubricated among members with a kicker, football and so on. Christine Weinzierl instructed me to use Matlab and simulating skills for the steady state analysis. Prashant Subhas Khadke always tried to relieve my stress with sharing common difficulties. Fabian Kubannek specially took care of me like a Korean friend with funny parties and entertainments. With respect to workshops, Mr. Uwe Herrmann, Mr. Wilfried Janssen and Ms. Nina Böge made experimental instruments and measuring devices for me. Ms. Ina Schunke helped me to submit every document to faculties or public services. Thanks to the institute members including above mentioned colleagues, my German life became wonderful and fruitful.

As well as TU Braunschweig, I do not want to miss the staffs in Magdeburg, Dr. Barbara Witter and Mr. Jürgen Koch as IMPRS coordinators. They helped me to settle down Germany softly and organised my IMPRS membership activity successfully. Thanks to also IMPRS members to share their own knowledge to solve scientific problems.

Acknowledgment

Lastly, I specially thank my families. Most of all, my lovely wife Na-Eun supported me all the time even though I lost my power to overcome many obstacles. She managed every tough problems wisely with her clever tactics. My son, Junho was brave and adventurous enough to overcome his foreign life. I owe plenty amount of my success to them. I am very grateful to my parents to growing and educated me up to accomplish high performance in the academic area. Finally, I thank my wife's family to advise me about German life and my brother to prop up the family enterprise.

Chapter 1

Introduction¹

1.1 Introductory explanation of fuel cells

Fuel cells are well known for environmental-friendly features compared to conventional engines or power plants. Fuel cells use natural gas, hydrogen or methanol as fuel, and produces less pollutants than other engines. Since Sir William Grove discovered the principle of fuel cells in 1842, many fuel cell types have been developed for different applications. For example, fuel cell electric vehicles are developed to satisfy newly strengthened regulation for clean environments. Some stationary fuel cell systems are already commercialized for certain applications: for larger applications, solid oxide fuel cells, molten carbonate fuel cells and phosphoric acid fuel cells are used as mid-size power plants or residential combined heat and power generators. Polymer electrolyte fuel cells are utilized in fuel cell powered electric vehicles or for portable uses [2, 3].

People want to use portable electric devices, such as smart phones, laptops or wearable devices for long operating time even though they are mostly limited to small volume and light weight. Humanoid robots are also restricted to use heavy batteries for high power and energy to operate autonomously [4]. Li-ion batteries can be a possible solution but only within the restrictions of certain operating ranges. As operating time of batteries is limited and insufficient, fuel cell systems can substitute or compensate for batteries due to their higher energy density [5]. To use fuel cells for portable applications, fuel cell systems need to be more compact and simpler to satisfy user requirements. Generally, low temperature operating fuel cells such as polymer electrolyte

¹Part of the results of this chapter was published in Youngseung Na, Federico Zenith, and Ulrike Krewer, *Energies*, 8(9):10409–10429, 2015.

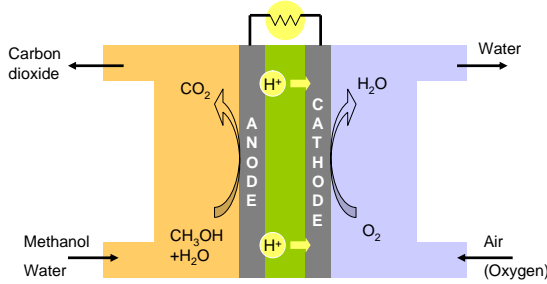
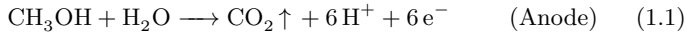


Fig. 1.1: Schematic diagram of direct methanol fuel cell

membrane fuel cells (PEMFC) and direct methanol fuel cells (DMFC) are selected for small scale applications because of their compactness [6].

Among polymer electrolyte fuel cells, direct methanol fuel cells are considered to be the most appropriate for portable applications because of their small size and the high energy density of methanol [7]. Compared to Lithium ion batteries [8], methanol has a 30 times higher energy density [9]. Besides, fuel cells need only a few seconds to swap fuel cartridges in contrast of several hours to recharge a battery.

The basic reactions in DMFCs are anodic and cathodic reactions as follows:



These reactions occur on catalyst surfaces contacting ionomer and reactants at each electrode as shown in Fig. 1.1. To supply the reactants to anode and cathode layers, actuators such as pumps or blowers are necessary. Particularly, a water recirculation system should be equipped within the portable application to dilute neat methanol. Otherwise as shown in Fig. 1.2a a large amount of dilute methanol solution within a big fuel tank is necessary and an almost same size of drain reservoir is also needed to exhaust liquid solution, which is only available in a laboratory [10]. Therefore, water as a product of reaction 1.2 is preferable to be reused as a reactant of reaction 1.1 to dilute

neat methanol in the mixer. Besides this water recirculation system, temperature control and concentration control systems are needed to optimize operating conditions for the higher efficiency. An example of a closed loop system is illustrated in Fig. 1.2b. The system consists of a DMFC stack, separators (a degasser and a condenser), a mixer, a methanol reservoir, a blower and two pumps. The blower supplies air to the cathode of the stack and the circulation pump supplies methanol solution to the anode. The unused air components are expelled from the stack into the condenser. The condensed water is recycled to the mixer which is mixed with the unused methanol solution from the degasser and neat methanol from the fuel reservoir. Actuators are controlled respectively by each controller. The detailed modelling of the system is reviewed in the next chapter.

1.2 State of the art

Fuel cell systems have been required to be efficient and compact for portable uses with autonomy and stability. First of all, autonomy and stability of systems should be satisfied for portable applications. A study on the conditions under which DMFC systems are autonomous, i.e. are able to maintain their water content without additional fresh water, was published by Zenith *et al.* [11], indicating how few critical variables influence that ability. Insightful experimental results on the dynamics of methanol concentration in DMFC systems were published by Ha *et al.* [12], who noticed the stabilising effect of methanol crossover. A complete analysis of dynamics and control in DMFC systems was later published by Zenith and Krewer [1], formalising the stability of the dynamics of methanol concentration and noting the metastability of the dynamics of water content, which requires feedback control. Next, a lot of research on membrane-electrode-assemblies [13], gas diffusion layers [14], other components [15] or stacks [16] has been carried out on optimization of design parameters to improve efficiencies. Kang *et al.* developed a solid electrolyte membrane to reduce methanol crossover [17] for high efficiency. An early steady-state study on pressurised DMFC systems was published by von Andrian and Meusinger [18], who noted that pressurisation of reactants increases the efficiency of a fuel cell. Specchia *et al.* [19] studied the positioning of a gas-liquid separator in the system layout, noting that it was necessary in some cases to feed fresh water to the system, and that this requirement de-

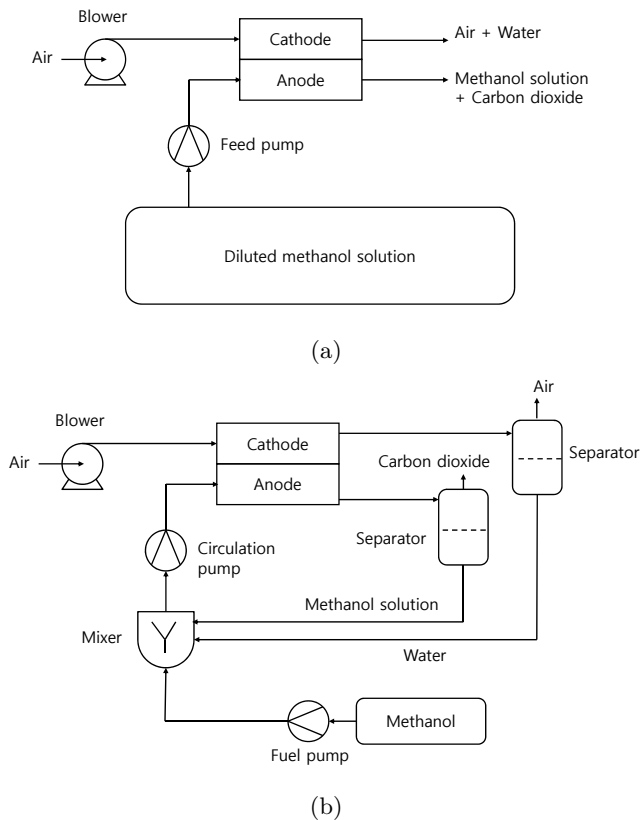


Fig. 1.2: Exemplary schematic diagram of (a) an open loop system and (b) closed system for DMFCs

creased with pressurisation. Besides efficiency, energy density is also a very important factor in portable systems [20], and it is therefore of interest to investigate the case in which some of the ancillary units are removed utilizing process integration, saving weight and size. Some of the systems reported in the literature are in fact overly complex, as they were thought more for stationary than portable power generation (e.g., von Andrian and Meusinger's layout features six heat-exchange units and five pumps). Dohle *et al.* [21] studied how system efficiency varied with respect to several parameters, confirming von Andrian and Meusinger's claim about pressurisation being detrimental to system efficiency. Last, despite the high energy density of methanol, DMFC systems are not very small because they need components like condensers to dilute methanol solution [22]. To shrink the system size, some researchers tried to omit system components such as fuel pumps. Passive type DMFC systems, which supply fuel without additional electric actuators. Kim *et al.* and Qian *et al.* [23, 24] developed a transport system which use pressurized carbon dioxide gas from the electrochemical reaction. For methanol transport, the pressurized carbon dioxide gas squeezes a methanol reservoir and methanol solution flows into the anode channels without additional pumps. Cao *et al.* developed an air breathing system to eliminate air pumps [25]. However, the passive systems have lower performance than active systems due to unstable and slower reactants supply, decreasing its power density [26].

1.3 Motivation and scope of this work

A portable DMFC system needs to be efficient and simple. Many researchers have investigated DMFC systems for decades to commercialize. However, the systems are still complex, and the influence of system variation on the performance is not well known yet. In this study, the variate systems are investigated for two purposes. One is for high efficiency with dynamic control, and the other one is for compact size with process integration. Simplicity may be obtained at the expense of efficiency or flexibility, and the task of this research is to illustrate the effects of system design and process integration on a generic DMFC system.

Advantages and disadvantages of the chosen systems are compared and quantified to suggest the appropriate areas of application for the system layouts. The main structure of this thesis is composed as follows:

- *Reference system* review and validation with experiments for direct methanol fuel cells (Chapter 2)
- Increasing faradaic efficiency of direct methanol fuel cell systems with separate tank and mixer using feedforward control of operating concentration (Chapter 3)
- Integrated direct methanol fuel cell systems minimizing fuel loss with dynamic concentration control for portable applications (Chapter 4)

The *reference system*, which is the base model of the variable systems in this study, is reviewed in detail in Chapter 2. The electrochemical and chemical reactions are defined with mass and energy balance equations. Besides the fuel cell itself, ancillary units are modelled one by one with relevant controllers. The feasibility envelope for the *reference system*, investigated by Zenith *et al.* [11], is validated experimentally for various temperatures and relative humidities in the climate chamber. After the steady state analysis, the dynamic behaviour of the *reference system* model is also fully validated with experiments while the autonomous operation with feedforward concentration control is partially validated without temperature controllers[27].

In Chapter 3, to improve faradaic efficiency, a *two-mixer system* and a *separate tank system* are introduced and compared with the *reference system*. The model of each system is also implemented with optimized controllers [28].

Lastly, to make the system compact for portable applications, processes in the system are integrated (Chapter 4). Coolers and separators are integrated at first to reduce the system size. Next the separator and the mixer are combined together. After this integration, the dynamic system behaviour is analysed and optimized for the higher efficiency with the algorithm that was obtained in Chapter 3.

Chapter 2

Reference system

The *reference system* as shown in Fig. 2.1 was taken as the base structure of this research because each actuator is controlled by its own controller - single-input and single output (SISO). The steady state model of the *reference system* has already been simulated by Zenith *et al.* [11] and the dynamic model was investigated by Zenith and Krewer [1]. These two models are mainly reviewed to compare experimental results with simulations. Most of all, each controller is derived from the fuel cell system models based on multicomponent equilibrium and thermodynamic equations which are introduced in the next section. The feedforward methanol controller of *reference system* was verified in Zenith *et al.* [27] but autonomous temperature control was omitted. Firstly, in this research the model at steady state is validated at various temperatures and relative humidities to identify feasibility envelopes of autonomous operation. Secondly, the dynamic behaviour is validated with an enhanced set-up from Zenith *et al.* [27] because heat loss on the whole system was much larger than heat generation from a DMFC stack, which was required to be heated by external electric heaters to keep the operating temperature 60 °C. This external heating set-up prohibited to validate the temperature control properly. For the purpose of bulk heat generation and effective heat insulation, a nine-cell DMFC stack was used in a climate chamber to validate autonomous operation.

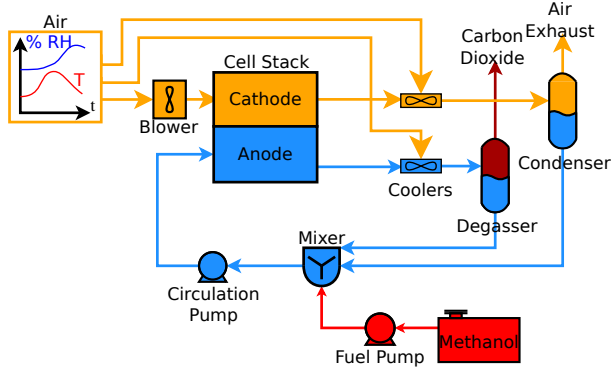


Fig. 2.1: The process layout of the *reference system* [1].

2.1 Review of modelling [1]

2.1.1 Multicomponent equilibrium

Five components, water, methanol, carbon dioxide, nitrogen and oxygen are taken into account for modelling. Each summation of gaseous mole fraction y_j and liquid mole fraction x_j is one for all components.

$$\sum_{j=1}^{\text{comp}} x_j = \sum_{j=1}^{\text{comp}} y_j = 1 \quad (2.1)$$

The mass balance of each species j and its total molar amount should be satisfied with overall molar fraction z_j :

$$z_j n = y_j n^{\text{gas}} + x_j n^{\text{liq}} \quad (2.2)$$

$$n = n^{\text{gas}} + n^{\text{liq}} \quad (2.3)$$

The multicomponent mixture is assumed to be in equilibrium. To calculate the multicomponent equilibrium, the Rachford-Rice [29] rela-

tions are derived by the vapour molar fraction $\beta = n^{\text{gas}}/n$.

$$\sum_{j=1}^{\text{comp}} (y_j - x_j) = 0 \quad (2.4)$$

Assuming that the solubility of carbon dioxide into methanol solution in the atmospheric pressure is negligible [19], only water and methanol are present in liquid phase. Carbon dioxide, nitrogen and oxygen are considered as incondensable components. The reduced number of components enables to simplify the equations with a second order polynomial. The vapour molar fraction β can be obtained by solving polynomials analytically using equilibrium constant $K_j = y_j/x_j$ [29].

$$x_j = \begin{cases} \frac{z_j}{1+\beta(K_j-1)} & j \in \{\text{CH}_3\text{OH}, \text{H}_2\text{O}\} \\ 0 & j \in \{\text{O}_2, \text{N}_2, \text{CO}_2\} \end{cases} \quad (2.5)$$

$$y_j = \begin{cases} K_j x_j & j \in \{\text{CH}_3\text{OH}, \text{H}_2\text{O}\} \\ \frac{z_j}{\beta} & j \in \{\text{O}_2, \text{N}_2, \text{CO}_2\} \end{cases} \quad (2.6)$$

The equilibrium constant K_j is estimated with the ratio of vapour pressure and total pressure with the activity coefficient γ .

$$K_j = \gamma_j \frac{p_j^{\text{sat}}}{p_{\text{env}}} \quad j \in \{\text{CH}_3\text{OH}, \text{H}_2\text{O}\} \quad (2.7)$$

The activity coefficient of methanol $\gamma_{\text{CH}_3\text{OH}}$ is not significantly influenced by temperature in the operating range of DMFCs and it was found that $\gamma_{\text{CH}_3\text{OH}}$ and $\gamma_{\text{H}_2\text{O}}$ can be assumed to be 2.15 and 1 respectively for diluted solutions [30].

2.1.2 Fuel cell

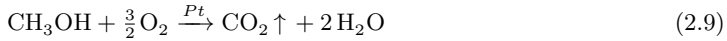
Zenith *et al.* [1] assumed that there is no material hold-up in the stack and the heat capacity of the stack is the sum of those of graphite plates excluding other components in the stack. The first assumption is valid when the internal volume of the reactants in the stack is relatively

smaller than that of the other volumetric components in the system. In this research, calculation of the stack heat capacity includes not only graphite plates but also clamping end plates and other components of the stack.

Besides, the published concepts in Zenith *et al.* [1] are incorporated with the current model in this work. From the electrochemical reaction 1.1, methanol reaction rate \dot{n}_r is directly determined by electric current I from Faraday's law [31]:

$$\dot{n}_r = \frac{NI}{6F} \quad (2.8)$$

where N is the number of cells in the stack and F is Faraday constant. A chemical reaction at the cathode side results from crossover methanol.



Methanol crossover results from diffusion between the catalyst layers of anode and cathode, where the methanol concentration at the cathode side $c_{\text{cl}}^{\text{cath}}$ is always assumed to be zero due to instantaneous oxidation:

$$\dot{n}_x = AN \frac{D}{d} (c_{\text{cl}}^{\text{an}} - c_{\text{cl}}^{\text{cath}}) \quad (2.10)$$

d and D are membrane thickness and diffusion coefficient respectively. The crossover flux \dot{n}_x can be related with diffusion from channel and electric current, using a steady state anode mass balance for methanol mass transfer coefficient k_m .

$$ANk_m(c^{\text{an}} - c_{\text{cl}}^{\text{an}}) = \frac{NI}{6F} + \dot{n}_x \quad (2.11)$$

Combining Equation 2.10 and 2.11 cancels out the anodic concentration term at catalyst layer $c_{\text{cl}}^{\text{an}}$. The crossover flux \dot{n}_x is rewritten as follows:

$$\dot{n}_x = N \left(\frac{k_m c^{\text{an}} A - \frac{I}{6F}}{1 + k_m d/D} \right) \quad (2.12)$$

where k_m is a function of temperature as in Scott *et al.* [32]. To simplify controllers, k_m is calibrated at a stack operating temperature of 60 °C. The coefficients \tilde{a} and \tilde{b} are considered as constant in controllers.

$$\dot{n}_x = N \left(\tilde{a} A c^{\text{an}} - \tilde{b} \frac{I}{6F} \right) \quad (2.13)$$

In DMFCs, methanol molecules drag water molecules through the membrane. The drag coefficient of the electro-osmosis k_d is calculated with the combination of the base value at 30 °C from Schaffer *et al.* [33] and the temperature dependency from Ren and Gottesfeld [34].

$$k_d = \left(4.2 + \frac{T^{\text{stack}} - 303.15K}{40K} \right) \quad (2.14)$$

Dragged water mole flow rate \dot{n}_d is proportional to current:

$$\dot{n}_d = N \cdot k_d \frac{I}{F} \quad (2.15)$$

For the mass balance of each species n_j , inlet and outlet mole flow rate $\dot{n}_{j,\text{in}}$ and $\dot{n}_{j,\text{out}}$ are calculated with an electrochemical reaction term and a crossover term.

$$\dot{n}_{j,\text{out}} = \dot{n}_{j,\text{in}} + \nu_j^s N \frac{I}{F} + \xi_j^s \dot{n}_x \quad (2.16)$$

The coefficients ν^s and ξ^s for each component j and side s (anodic or cathodic) are listed in Table 2.1.

The temperature of the stack T^{stack} is determined by the energy balance of inlet and outlet enthalpies with the heat capacity C_p , being calibrated by experiment.

$$C_p \frac{dT^{\text{stack}}}{dt} = \sum_{j,s} h_j(T_{\text{in}}^s) \dot{n}_{j,\text{in}}^s - \sum_{j,s} h_j(T^{\text{stack}}) \dot{n}_{j,\text{out}}^s - UI \quad (2.17)$$

The voltage and current relationship is assumed as Thévenin equivalent circuit for the simplicity because this research focuses on the

Table 2.1: The stoichiometric coefficients for main reaction ν_j^s and crossover ξ_j^s for each species on cathode and anode.

j	CH ₃ OH	H ₂ O	O ₂	CO ₂	N ₂
ν_j^{an}	-1/6	-1/6 - k_d	0	1/6	0
ν_j^{cath}	0	1/2 + k_d	-1/4	0	0
ξ_j^{an}	-1	0	0	0	0
ξ_j^{cath}	0	2	-3/2	1	0

system control not the fuel cell modelling itself. The overall resistance R , including anode and cathode over potential, is assumed to be linear in the range of the cell voltage from 0.3 V to 0.5 V.

$$U = U_0 - RI \quad (2.18)$$

where U_0 is open circuit voltage of the DMFC.

2.1.3 Coolers

Downstream of anode and cathode outlet, coolers remove heat from the exhausted products. The amount of heat dissipation is determined by the outlet temperature T_{out} of the cooler, which is controlled by the set temperature \bar{T} . Cooler outlet temperature is constrained within the range of cooler inlet temperature T_{in} and environmental temperature T^{env} . The process of the cooler is assumed to be first order lag with time constant $\tau = 120s$ as in Zenith *et al.* [1]. The Laplace form of the process with variable s follows:

$$T_{\text{out}} = \frac{1}{\tau s + 1} \min \left(\max(\bar{T}, T^{\text{env}}), T_{\text{in}} \right) \quad (2.19)$$

2.1.4 Separators

A degasser and a condenser separate the two phase flow from anode and cathode outlet respectively as shown in Fig. 2.2. All incondensable components such as nitrogen, oxygen and carbon dioxide pass through

separators without any liquefaction. Condensible components such as water and methanol split as gaseous and liquid phase. The vapour molar fraction β of the mixture is determined by Rachford-Rice equation discussed in section 2.1.1. Mole fraction $\dot{n}_{in,j}$ and equilibrium constant K_j of each component determine the mole fractions of gas and liquid phase components.

$$\dot{n}_{out,j}^{gas} = \dot{n}_{in,j} \quad j \in \{O_2, CO_2, N_2\} \quad (2.20)$$

$$\dot{n}_{out,j}^{gas} = \dot{n}_{in,j} \frac{\beta K_j}{1 + \beta(K_j - 1)} \quad j \in \{CH_3OH, H_2O\} \quad (2.21)$$

$$\dot{n}_{out,j}^{liq} = \dot{n}_{in,j} - \dot{n}_{out,j}^{gas} \quad \forall j \quad (2.22)$$

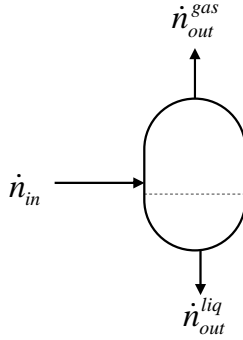


Fig. 2.2: The block diagram of gas-liquid separator in fuel cell systems

2.1.5 Mixer

It is assumed that only the mixer holds up materials in the system because the material hold-ups of the other components are negligible due to their significantly smaller size in Zenith *et al.* [1]. The mixer is considered as ideally stirred tank reactor to blend mixture perfectly as shown in Fig 2.3. Accumulating material and energy are determined

by the summation of all entering and exiting flows as follows:

$$\frac{dn_j^{\text{mix}}}{dt} = \sum_{\text{flows}} \dot{n}_j^{\text{flows}} \quad (2.23)$$

$$\frac{dE^{\text{mix}}}{dt} = \sum_{\text{flows}} \dot{h}_j^{\text{flows}} \quad (2.24)$$

where j means the species and flows the connected flows to the mixer.

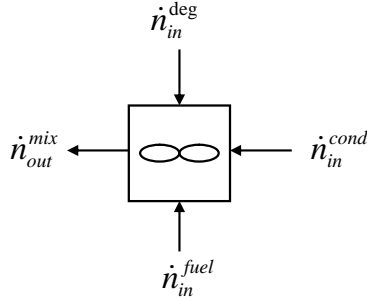


Fig. 2.3: The block diagram of mixer in the *reference system* of direct methanol fuel cells

2.1.6 Controllers

The direct methanol fuel cell system needs to control cathodic air inlet flow $\dot{V}_{\text{in}}^{\text{cath}}$, solution volume in the mixer V^{mix} , stack temperature T^{stack} , methanol concentration $c_{\text{out}}^{\text{an}}$ and anodic solution flow \dot{V}^{sol} . For these controllers I used the algorithm from Zenith *et al.* [1] at Table 2.2. First of all, feedforward control is suitable for cathodic air inlet flow $\dot{V}_{\text{in}}^{\text{cath}}$ with air excess ratio λ^{cath} because the time constant of changes in oxygen mole fraction y_{O_2} in the cathode is small within the range

Table 2.2: Summary of the proposed controllers for the reference DMFC system

Controlled variable	Manipulated variable	Measurements	Type
y_{O_2}	\dot{V}_{in}^{cath}	I	Feedforward
V^{mix}	\bar{T}^{cond}	$V^{mix}, T^{cond}, \dot{n}_{in}^{cath}$	Nonlinear-gain
T^{stack}	T^{deg}	T^{stack}	P feedback
c_{out}^{an}	$\dot{n}_{CH_3OH}^{fuel}$	I	PID feedback
λ^{an}	\dot{V}^{sol}	I	Feedforward

of several seconds, and the disturbing variables such as current I are measurable.

Next, solution volume in the mixer and stack temperature are controlled by a feedback controller using an algorithm with measured variables such as V^{mix} and T^{stack} . For the accurate control of the concentration at inlet and outlet of the anode channel, feedback control is preferred. But for the highly precise methanol sensors such as density meters or refractometers are not suitable for the portable system due to their size and slow response time [12]. Therefore the concentration control uses feedforward control based on the fuel cell model.

Lastly, the anodic solution flow \dot{n}_{in,CH_3OH}^{an} is controlled by ratio control algorithm with excess ratio λ^{an} and measured current to keep the mole flow ratio of methanol anodic inlet to the replenished methanol from the fuel reservoir.

2.1.6.1 Air flow

The amount of consumed oxygen at the cathode is related with electrochemical reaction and methanol oxidation from methanol crossover, which are proportional to current and concentration respectively. The methanol concentration is not measurable in the system, therefore a maximal estimated concentration of $\hat{c}^{an} = 1100 \text{ mol/m}^3$ is used. As discussed in the last section, the parameters \tilde{a} and \tilde{b} are calibrated at the operating temperature 60°C , and are fixed as constant values in the controller. The volume flow rate of the air \dot{V}_{in}^{cath} is calculated by

the ideal gas law with gas constant R , environmental pressure p^{env} and oxygen mole fraction $y_{\text{O}_2}^{\text{env}}$. The excess ratio λ^{cath} is fixed as 3 which means that oxygen is supplied three times more than actual consumption to prevent oxygen depletion at the whole catalyst layer as a rule of thumb. This yields the following feed forward control [1].

$$\dot{V}_{\text{in}}^{\text{cath}} = \lambda^{\text{cath}} N \frac{RT^{\text{env}}}{p^{\text{env}} y_{\text{O}_2}^{\text{env}}} \left(\frac{1 - \tilde{b}}{4F} I + \frac{3}{2} \tilde{a} A \hat{c}^{\text{an}} \right) \quad (2.25)$$

2.1.6.2 Water recovery

To guarantee recycling of a sufficient amount of water to the anodic loop, a scheduled gained proportional controller (feedback P-controller) is employed. Water condensation in the condenser is determined by the condenser temperature T^{cond} and saturated pressure $\pi_{\text{water}}(T^{\text{cond}})$, which is estimated by Antoine Equation 2.26 [35].

$$\pi_{\text{water}}(T^{\text{cond}}) = 10^{5.20409 - \frac{1581.341}{T^{\text{cond}} + 33.50}} \times 10^5 \quad (2.26)$$

where the operating temperature is within 255.8 K to 373 K. As a change in the condenser temperature leads directly to a change in liquid volume V^{mix} in the mixer in Equation 2.27.

$$\delta \tilde{T}^{\text{cond}} = \left[\tau_c \frac{\dot{n}_{\text{in}}^{\text{cath}}}{p^{\text{env}}} \frac{d\pi_{\text{water}}(T^{\text{cond}})}{dT^{\text{cond}}} \right]^{-1} \frac{\rho_{\text{water}}}{M_{\text{water}}} \delta V^{\text{mix}} \quad (2.27)$$

The differentiated Antoine equation is used as a scheduled gain of the P controller as shown in Fig. 2.4.

2.1.6.3 Stack temperature

Typically the stack temperature is controlled by adjusting loop solution temperature in DMFC systems while PEMFC systems control the stack temperature directly with cooling channels in the stack. When the stack temperature is set to 60 °C and passes through the mixer without cooling, the inserted neat methanol in the mixer evaporates immediately. To prevent methanol evaporating, the anodic solution should be cooled down before entering the mixer. The temperature

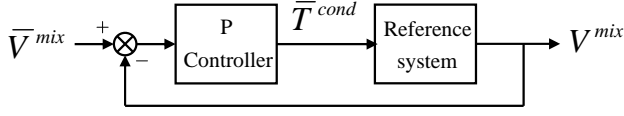


Fig. 2.4: The block diagram of P controller for water recovery in the condenser

change of the degasser T^{deg} controls the stack temperature T^{stack} with PID feedback controller.

$$\bar{T}^{\text{deg}} = T_o^{\text{deg}} + k_c \left(e + \frac{1}{\tau_I} \int e dt + \frac{de}{dt} \tau_D \right) \quad (2.28)$$

where $e = \bar{T}^{\text{stack}} - T^{\text{stack}}$.

The response time of the cascade controller for the cooler is assumed to be 120 s as Zenith and Krewer [1]. According to Skogestad's method [36], the parameters k_c , τ_I and τ_D are determined to be 0.625, 75 s and 60 s respectively.

2.1.6.4 Fuel flow

The necessary amount of methanol feed for the system $\dot{n}_{\text{CH}_3\text{OH}}^{\text{fuel}}$ is obtained by summing up the methanol consumption in the electrochemical reaction and methanol oxidation from crossover. The representative methanol concentration in the anode side c^{an} is assumed to be the outlet concentration $c_{\text{out}}^{\text{an}}$ while the concentration c^{mix} in the mixer equals the inlet concentration $c_{\text{in}}^{\text{an}}$. Methanol evaporation in degasser, which is realised to be small in Zenith *et al.* [37] is eventually neglected in the reference system.

$$\dot{n}_{\text{CH}_3\text{OH}}^{\text{fuel}} = N \left(\frac{1 - \tilde{b}}{6F} I + \tilde{a} A \bar{c}_{\text{out}}^{\text{an}} \right) \quad (2.29)$$

where the parameter \tilde{a} and \tilde{b} are same for Equation 2.25.

2.1.6.5 Solution volume flow

As visible in Fig. 2.1, anodic solution is circulated in the anodic loop passing through the cooler and degasser. Neat methanol from the reservoir is replenished to the anodic loop for the compensation of consumed methanol in the anodic loop. The methanol mole flow of anode inlet $\dot{n}_{\text{in},\text{CH}_3\text{OH}}^{\text{an}}$ is controlled by the anodic excess ratio λ^{an} to the supplemented methanol mole flow $\dot{n}_{\text{CH}_3\text{OH}}^{\text{fuel}}$ as follows:

$$\dot{n}_{\text{in},\text{CH}_3\text{OH}}^{\text{an}} = \lambda^{\text{an}} \cdot \dot{n}_{\text{CH}_3\text{OH}}^{\text{fuel}} \quad (2.30)$$

The excess ratio λ^{an} of the fuel supply is known to be two to three for stable operation of DMFC systems [16]. The solution volume flow rate \dot{V}^{sol} is calculated with the methanol concentration in the mixer c^{mix} and mole flow $\dot{n}_{\text{in},\text{CH}_3\text{OH}}^{\text{an}}$. However, in this research no concentration sensor is used for control. Therefore, the minimally estimated concentration \tilde{c}^{mix} in the mixer substitutes it. Rearranging equation with Equation 2.29 yields the solution flow rate follows.

$$\dot{V}^{\text{sol}} = \frac{\lambda^{\text{an}} N}{\tilde{c}^{\text{mix}}} \left(\frac{1 - \tilde{b}}{6F} I + \tilde{a} A \tilde{c}_{\text{out}}^{\text{an}} \right) \quad (2.31)$$

2.2 Experiment

Depending on purposes, experimental set-ups are slightly different from each other. For steady state analysis of the *reference system*, an air pump supplies cathodic reactants from a climate chamber at the same temperature and relative humidity condition of the other components such as a degasser or a condenser in the climate chamber. In contrast, a mass flow controller is used for dynamic analysis because it can supply air precisely even though water droplets disturb air flow according to variable current disturbance. The other difference of the set-up between steady state analysis and dynamic analysis is the temperature control of the stack. The main purpose of steady state analysis is investigating water accumulation at static conditions depending on variables such as stack temperature, flow rates and so on. In this sense, using electric heater to heat up the stack is more reliable than controlling solution temperature to adjust stack temperature by heat exchanger.

So a 3-cell stack, which generates little amount of heat, is employed for steady state analysis. However, self-generated heat from reactions in the stack should be measured and investigated in dynamic analysis to investigate autonomous operation of the *reference system*. Therefore, a 9-cell stack with larger heat generation is utilized for analysis without need for electric heaters. Detailed specifications are introduced in the next section.

2.2.1 System components

To validate the *reference system* with experiments, the DMFC system is set up in a climate chamber (Fig. 2.5). The devices which are insensitive to the environmental temperature such as electric load, power supply and mass flow controllers are placed outside of the climate chamber (MKF240, Binder, Germany).

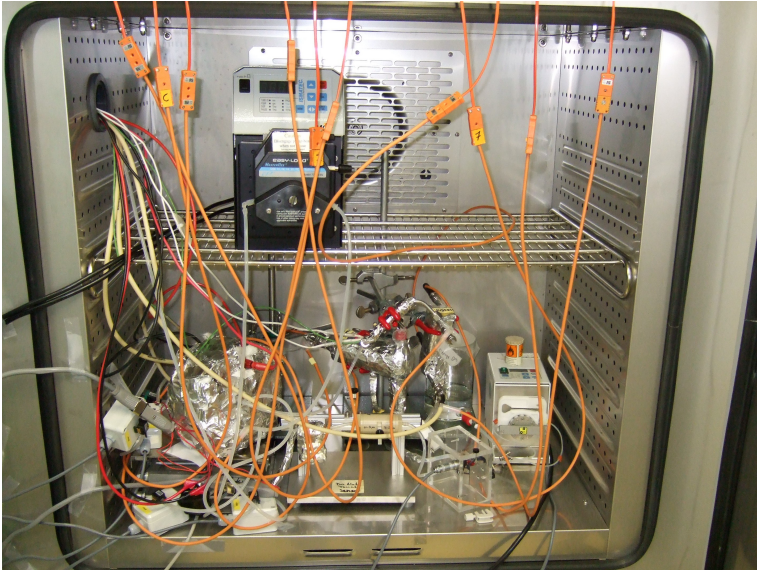


Fig. 2.5: The *reference system* of the direct methanol fuel cell in the climate chamber

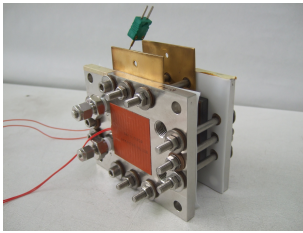
The in-house designed components are shown in Fig. 2.6. The DMFC stack shown in Fig. 2.6a has three cells made of Nafion N115 (Type MEA0281, Johnson Matthey, UK) with 26 cm^2 active area. Two plate heaters (HR5417R, Minco, Germany) with each $5.3\ \Omega$ is glued to both end plates of the stack. On the contrary, for dynamic analysis, another fuel cell stack (15 W DMFC stack, balticFuelCells, Germany) is used, which is composed of 9 cells with an active area of 31.5 cm^2 per cell. Stack temperature is measured with a K-type thermocouple, 50 mm deep inside of the middle bipolar plate. The fuel cell system for dynamic analysis is placed in a climate chamber (PL-3KPH, ESPEC, Japan) to control the starting and ambient temperature.

Insulated K-type thermocouple probes measure temperatures of liquid preventing corrosion from direct contact with acidic solution, while R/S-type thermocouples with a T-shape casing as shown in 2.7 are employed for the gas phase.

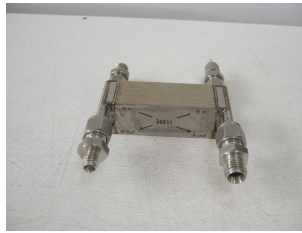
The anodic cooler (IMM, Germany) in Fig. 2.6b has 230 cm^2 heat exchanging area and heat transfer coefficient of $188\text{ W/m}^2\text{K}$. The cathodic cooler (HX/C-301, IMM, Germany) with heat transfer coefficient of $82\text{ W/m}^2\text{K}$ and the area of 246 cm^2 is serially connected with the condenser in body (Fig. 2.6e) to separate gas and liquid by gravity. The degasser (Fig. 2.6c) made of glass has three holes which are connected to the anodic cooler, the mixer and the environment. To remove cations from the solution, an ion exchanger as shown in Fig. 2.6d (Amberlyst 15, Merck KGaA, Germany) is employed in a PEEK container between glass filters (VitraPOR P16, ROBU, Germany) which block particles against damaging the sensitive density meter. Methanol concentration is measured on-line by a density meter (MCS, ISSYS, USA) to monitor the accuracy of feedforward controllers.

The mixer is designed in-house with a strain gauge (FSH01483, Futek, Germany) to weigh the solution weight in the mixer, which has an inner volume of 10 cm^3 (Fig. 2.8).

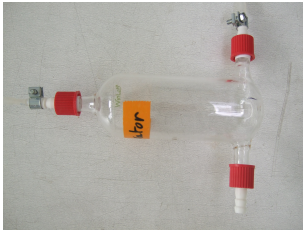
The other ready-made devices follow: Mass flow controllers (Smart-Trak C100, Sierra, USA) supply air to the cathode and the anode and cathode coolers, while an air pump (NMP05b, KNF, Switzerland) supplies cathode reactants at steady state analysis. The tubes in contact with liquid phases are Tygon 3350, whereas the others are A-60-G Norprene. To minimise additional heat loss on the surface of coolers, they are insulated with glass fibre and aluminium foil. The solution flow is set by a larger peristaltic pump (MCP Standard, Ismatec, Switzer-



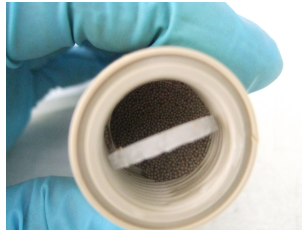
(a) DMFC stack



(b) Anodic cooler



(c) Degasser



(d) Ion exchanger



(e) Condenser

Fig. 2.6: Taylor made components in the direct methanol fuel cell system

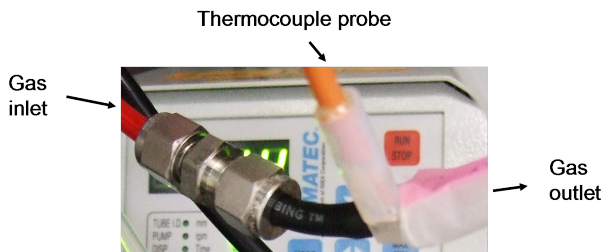


Fig. 2.7: T-shape casing of a thermocouple probe for measuring gas temperature

land) with an Easy-Load pumping head; the flows from fuel and water tank are set by smaller peristaltic pumps (Reglo Digital, Ismatec, Switzerland). Electric current is manipulated, and voltage is measured by an electric load (ZS512-4SV20NV, Höcherl & Hackl, Germany). All controllers and measurement devices communicate with real-time LabVIEW hardware (cRIO-9072, National Instruments, USA), programmed in-house.

2.2.2 Setup for steady state analysis

To operate the DMFC system without extra water supply - in the following called 'autonomous operation' - sufficient amount of water vapour should be condensed for dilution of the methanol concentration, otherwise the system loses the controllability of the methanol concentration. The maximum amount of condensing water in typical DMFC systems is accomplished at the lowest temperature of the cooler, which is equal to the environment temperature. Feasibility envelopes of DMFC systems for autonomous operation are simulated by Zenith *et al.* [11] with ideal assumptions such as the same temperature between environment and coolers. To validate the simulation results at the ideal conditions, all system components are installed in the climate chamber and kept at the set temperature except the stack. The stack temperature retained at 60 °C as in the simulations by the aforementioned electric heaters.

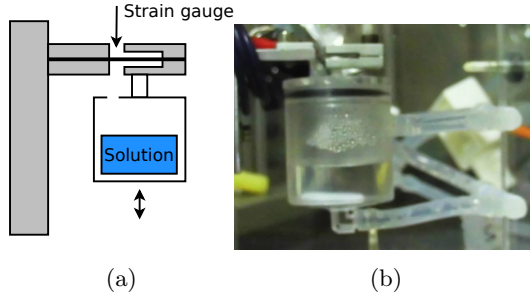


Fig. 2.8: (a) The sketch of the weighing mechanism of a tank with the strain gauge and (b) the picture of the actual mixer attached to the strain gauge.

2.2.2.1 Operating procedure

The feasibility envelope for autonomous operation of the *reference system* is obtained in experiments and compared with simulation results. The contour graph of feasibility envelope is drawn in the range of the environmental temperature from 27 °C to 57 °C with intervals of 5 °C and environmental relative humidity from 20% to 90% with 10% intervals in the experiment. Water accumulation rate is measured at all 49 conditions as shown in Fig. 2.9 to evaluate if sufficient water is available at each condition. In addition, sensitivity studies were conducted with variation in air excess ratio λ^{cath} , stack current I and condenser temperature T^{cond} , as given in Table 2.3. No.1 is the reference condition. At condition No.3, the condenser is heated by electric heater to keep the temperature 10 °C higher than ambient in the climate chamber. The stack is always heated up by the plate heater up to 60 °C to fully activate reaction kinetics in fuel cells. At preconditioning, the system was heated up to set environmental temperature and relative humidity condition in the climate chamber. After reaching set temperature and relative humidity, the system is kept for 30 minutes at the condition to stabilize the temperatures of all components. The electric load is set according to Table 2.3. Cathodic air flow rate is controlled by the excess ratio of lambda λ^{cath} (Equation 2.25). The solution flow rate in the anodic loop is determined by excess ratio of 3 according to Equation

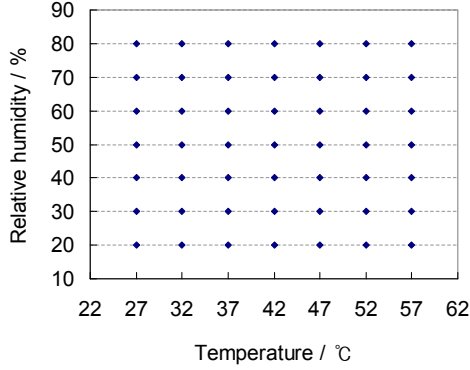


Fig. 2.9: Grid map for setting temperature and relative humidity in the climate chamber

Table 2.3: Operating conditions for steady state analysis of the DMFC system

No.	λ^{cath}	I	$T^{\text{cond}} - T^{\text{env}}$
1 ^{ref}	5	2A	0°C
2	10	2A	0°C
3	5	2A	+10°C
4	5	1A	0°C

2.31. After preconditioning with temperature and concentration, solution weight is measured for 30 minutes to calculate the accumulating rates of water.

2.2.3 Setup for dynamic behaviour analysis

The limiting environmental conditions for autonomous operation are identified with steady state analysis. When fuel cells are applied in actual devices, electric current can change dynamically. In spite of dynamic disturbances, DMFC systems also should operate autonomously and reliability. The control strategy for autonomy is proposed by Zenith

and Krewer [1]. In this section, the system model is validated, and the feasibility of assumptions in the model is evaluated.

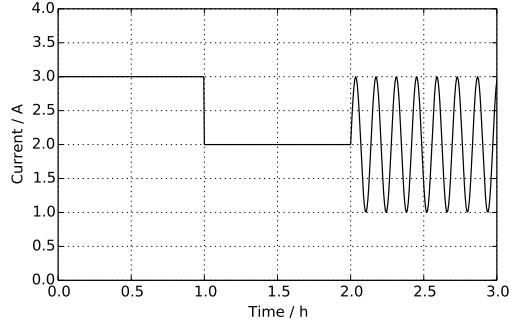


Fig. 2.10: Input current to all DMFC systems with 9 cells and 30 cm² as an active area

2.2.3.1 Operating procedure

To evaluate the system model, assumptions such as perfect insulation of system components in the model are required to be also realized in the experiment. Two effective methods to reduce additional heat loss are insulating components and equalizing surrounding temperature with that of system components. First one is accomplished by wrapping components with glass fibre cotton and aluminium foil to minimize heat transfer between the system and environment. The other is setting the surrounding temperature as the initial temperature 37 °C at the beginning of experiments. While warming up the system, the concentration of the solution is stabilized in the anodic loop for about one hour. During stabilization of methanol concentration in the anodic loop, the methanol crossover results in heating up the stack to around 45 °C.

When temperature keeps constant for an hour, the climate chamber shut down to avoid disturbing evaluation of the temperature controllers of the system. In the simulation, heat is assumed to transfer only between reactants and coolant fluid. After this preconditioning of tem-

perature and concentration, the current profile as shown in Fig. 2.10 is applied to the system as a disturbance load, which is composed of three regions as start up, stepping down and oscillating. During start up, 3 A is drawn for one hour. Next, the current is stepped down to 2 A; after maintaining 2 A for another hour, a sinusoidal profile is added to the current profile, with an amplitude of 1 A and a period of 500 s. For 3 hours, the control schemes presented in the previous sections are realized in the controlling program to validate the simulation, and data are logged via LabVIEW software once a second.

2.2.4 Potential error analysis

The concentration sensor functions by measuring the density of liquid solution in the anodic loop. The producer guarantees an accuracy of $\pm 0.30\%$ in the operating range between 0 to 10 %_w, which corresponds to about ± 0.1 M up to 3 M. The operating concentration of this study is between 0.5 M to 2 M, well within the validity range.

The voltage signal accuracy of the strain gauge is $\pm 0.25\%$ of rated output voltage at room temperature; if the temperature changes, the error increases with $\pm 0.036\%/K$. In this study, to reduce the error from temperature variance, the mixer is located in an additionally insulated air-filled case.

The electric load has the input error range $\pm 0.02\%$ of voltage signals and monitoring voltage-offset of ± 15 mV.

A K-type thermocouple has a temperature error of ± 1.5 K, while an R/S type thermocouple has ± 1.0 K.

2.3 Results and discussion

2.3.1 Steady state analysis

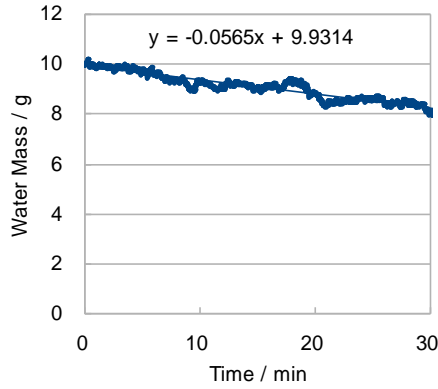
The water accumulation data in the mixer were collected at all conditions given in Table 2.3 and all temperatures and relative humidities given in 2.9. Using linear regression yields a water accumulation rate for each case. For example, the slope of the graph at 57°C of operating temperature and 20% of relative humidity is negative as seen in Fig. 2.11a while the one at 57°C and 90% is positive (Fig. 2.11b). The observed accumulation and depletion of water in the system shows the

high dependency of feasibility for autonomous operation on environmental conditions. The contour graph with the regressed accumulation rates for all relative humidities and temperature are plotted in Fig. 2.12 for the experimental conditions 1 and 2 of Table 2.3.

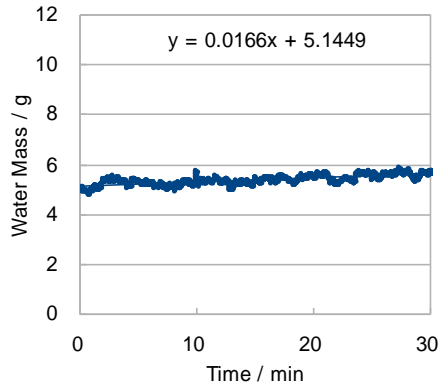
In the three-dimensional graph, the area below the blue plane corresponds to the depletion of water. At the high temperature and low relative humidity region, the system would dry out. Obviously at the top left side, corresponding to cold and wet region, water is recovered at the highest rate. With respect to the experimental condition No.1 in Table 2.3, the peak recovery rate reaches almost 0.06 g/min (Fig. 2.12a) which may cause overflow in the mixer due to low evaporation.

Water is depleted over a significantly wider range of temperature and relative humidity when the system is operated at a high excess ratio of cathode air supply as shown in Fig. 2.12b. The more air is exhausted out of cathode, the more water vapour evaporated in the condenser.

To compare the results with the simulation of Zenith *et al.* [11], the feasibility envelopes for autonomous operation of the system which are the boundary in between water accumulation and depletion for a given set of operating conditions, are plotted in Fig. 2.13 for experiment and simulation. The feasibility envelopes from the experiments are not smooth because they are extracted from the estimated contour graph. Despite the coarse contour, the trend of the feasibility envelope at high excess ratio fits with simulation results Fig. 2.13a. The feasibility envelope at higher condenser temperature condition (Fig. 2.13b) also shows good agreement but is slightly shifted to the right side because the temperature of the condenser is measured on the surface of it, not inside. The temperature of the heated surface by heating plates is expected to be higher than inside. At low relative humidity condition such as 20% and higher temperatures than 300 K, the DMFC system cannot operate autonomously with condition No. 2 and 3 as shown in Fig 2.13a and 2.13b. However, at high relative humidity condition such as 90% and high excess ratio condition (No. 2), the system operated autonomously until at 330 K because almost fully saturated air from inlet prevented water evaporation in the condenser. If the anodic cooler is not possible to cool down the condenser temperature close to the environmental temperature, the system needs extra water supply even in high relative humidity condition as shown in Fig. 2.13b. Lastly, a change in current does not have significant impact on the feasibly operating range (Fig. 2.13c) as same as in simulation. It can be concluded that at steady

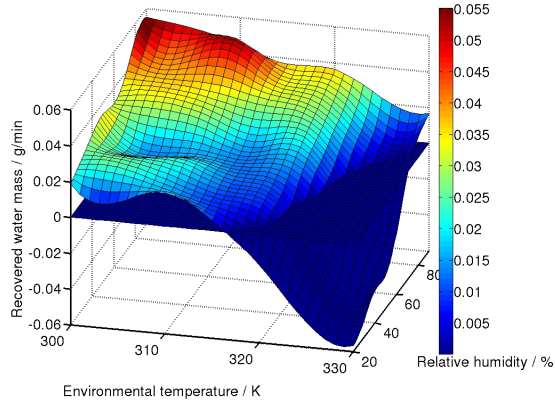


(a) rH=20%

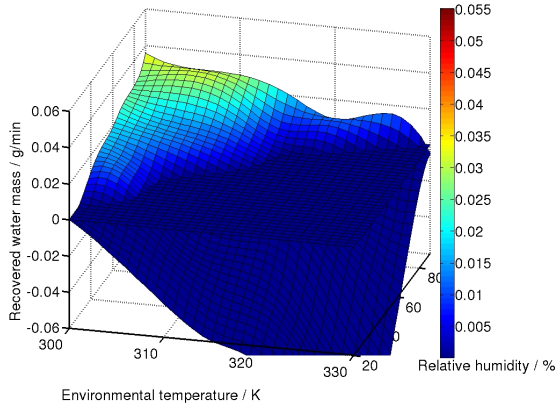


(b) rH=90%

Fig. 2.11: Water accumulation during constant current operation of the *reference system* at different relative humidity of 20% (a) and 90% (b) at a temperature of 57°C



(a)



(b)

Fig. 2.12: Water accumulation during constant current operation of the *reference system* at (a) condition 1 and (b) 2 in Table 2.3 and plane at 0 to denote stable water level

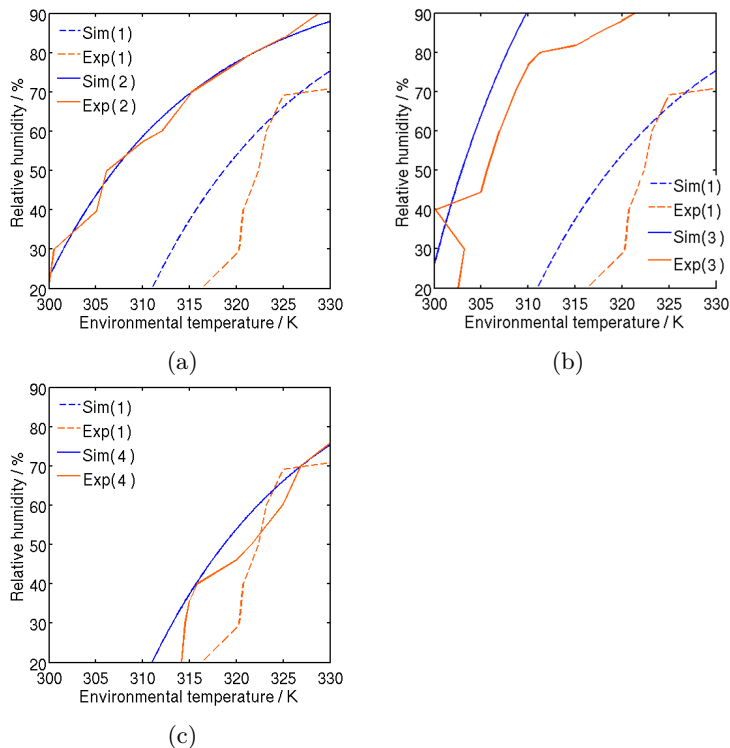


Fig. 2.13: Feasibility envelopes for the autonomous operation of the *reference system* at condition 1 with those (a) at condition 2, (b) at condition 3 or (c) at condition 4 in Table 2.3

state, the feasibility envelopes in various conditions in simulation are successfully validated with measuring water accumulation of the system in the climate chamber. The fuel cell system model is evaluated with experiments for analysing dynamic behaviour in the next section.

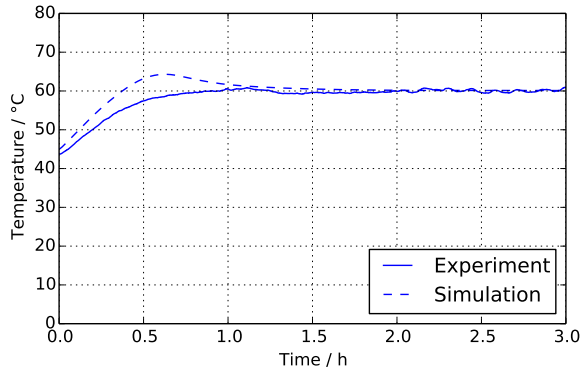


Fig. 2.14: The temperature profile of the stack in the *reference system*

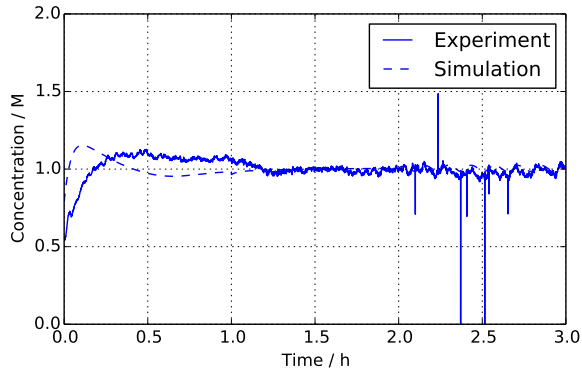


Fig. 2.15: Outlet concentration profile in the anodic loop of the *reference system*

2.3.2 Dynamic behaviour analysis

The control strategies for stack temperature, methanol concentration in the anodic loop, and water recovery are evaluated by analysing the response to aforementioned current disturbance in Fig. 2.10 for dynamic analysis. Results are shown in Fig. 2.14 and Fig. 2.15. At the beginning, the temperature profile of the simulation is found to be slightly higher than that of the experiment because the system components such as the condenser or coolers are assumed to have no heat capacities in the simulation as shown in Fig. 2.14. The larger heat mass of the corresponding experimental components results in slower convergence of stack temperature to the set temperature than in the simulation. Still dynamic load operation did not affect experiment and simulation.

The initial concentration in the mixer is set to 1.0 M. The concentration profile in Fig. 2.15 is measured at the outlet of the degasser after separation of the gas components. Application of the feedforward controller to the *reference system* leads to deviations in the concentration of simulations and experiments within ± 0.1 M during the first hour. The concentration overshoot at the beginning of the simulation does not appear in the experimental results because liquid solution doesn't exist only in the mixer, but also in the other components such as the stack, coolers, separators or tubes. The additional liquid solution in these reservoirs in experiments slowed down convergence to the set concentration.

After the peak of the concentration profile in the simulation, methanol concentration fell below the set concentration of 1.0 M because methanol crossover occurred more than estimation due to the high temperature of the stack during the period. In contrast, a lower temperature of the stack during start up than the set temperature mitigated methanol crossover in the experiment. Therefore the concentration became higher than the set value because the parameters \tilde{a} and \tilde{b} are calibrated at 60 °C. Due to the overestimated parameters, more fuel was supplied than the necessary amount to keep concentration stable. Therefore the concentration profile of the experiment is higher than the set concentration during the second half hour. At the rest of the period, concentration converged to the set value in both, simulation and experiment, controllers can, therefore, compensate at dynamic load operation.

The solution weight profile in the mixer in the experiment fluctuates more vigorously than that in the simulation as shown in Fig. 2.16. The difference between simulation and experimental results are caused

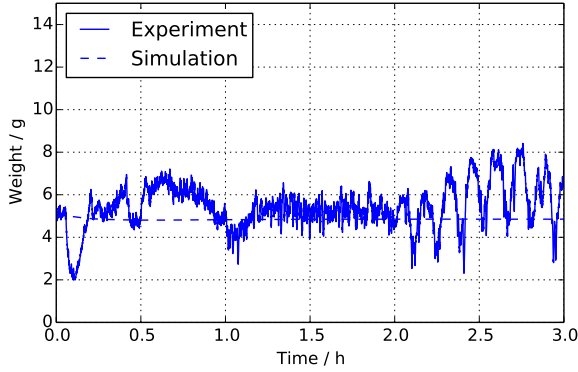


Fig. 2.16: Solution weight during operation of the mixer in the *reference system*

by three different regimes. First, the high-frequency oscillation results from the unstable measurement of weight with the strain gauge, which is influenced by liquid droplets from tanks such as the degasser and the condenser. Second, during the first half hour, the massive cooler needed time to be heated up, and water was condensed more than set by the controller due to low temperature. After the cooler was fully heated, more water evaporated than produced, and the solution weight in the mixer decreased to the set value of 5 g. When the current changed to low current, less water was produced than at high current. So the condenser was controlled to be cooled down immediately, and solution weight was stabilized for an hour before sinusoidal current disturbance. Last, the deep valleys at the beginning and 0.5 hours later are attributed to unexpected flow stagnation in small size tube between the degasser and the mixer. At the liquid outlet of the degasser, unseparated gas bubbles may block the liquid flow until certain amount of liquid flushing out solution to the mixer. Then the liquid level in the mixer is recovered.

2.4 Conclusions

In this section, the simulation results of the dynamics and feasible operating frame for autonomous operation are compared with experiments. In the simulation, the feasibility envelopes are investigated by calculating the steady state equations for the zero water accumulation. On the contrary, in the experiment, after determining a water accumulation rate for each condition, the feasibility envelope is obtained by interpolation. The experiments matched successfully with the simulation results. In this sense, with the comparison, the feasibility envelopes from the simulation are well validated by experiments. The dynamic behaviour is also successfully simulated with temperature and concentration except water accumulation. Temperature and concentration are controlled within the acceptable error ranges. The model is thus capable of capturing most of the phenomena of interest and can be used in the following to simulate and evaluate various system configurations of fuel cells.

Chapter 3

System variation for high efficiency²

The concept of this chapter is intrigued from the research of Arisetty et al. [38], which showed that an optimal methanol concentration exists in a DMFC leading to maximum faradaic efficiency. To quantify the implications of this finding on the design of autonomously operating systems, two different DMFC system designs are developed and compared.

A *reference system* where each component serves only one function (see Fig. 2.1) has been investigated by Zenith and Krewer [1] and in Chapter 2. In that system, the recycled solution from the degasser and the recycled water from the condenser are collected and are joined with neat methanol in a relatively large mixer to mitigate concentration fluctuation. The well-blended solution from this mixer is then supplied to the anode inlet of the DMFC stack. Since the dynamics of methanol concentration in the anodic loop is stable, it is possible to control it without measurement or feedback: this concept also has been validated in experiments with feedforward control of a concentration in Chapter 2: the controller with the *reference system* was shown to be able to maintain a constant concentration during operation. However, the *reference system* cannot change the concentration rapidly, because of the slow concentration transients in the large mixer; in particular, it cannot promptly adapt the concentration to the stack current. In this chapter, two different system designs are shown to be able to control concentration more rapidly, and thereby attain greater efficiency in accordance to the findings of Arisetty et al. [38]. Mathematical models

²Part of the results of this chapter was published in Youngseung Na, Federico Zenith, and Ulrike Krewer, *Energies*, 8(9):10409–10429, 2015.

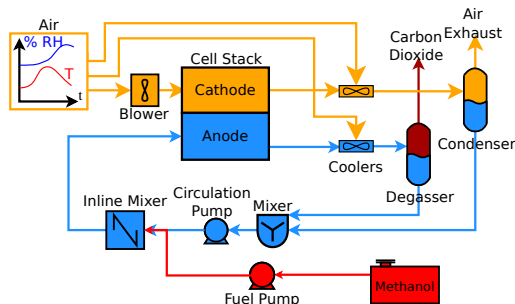


Fig. 3.1: The process layout of the *two-mixer system*.

of these systems, including peripheral devices, were implemented in a dynamic simulation of the model and validated experimentally.

3.1 System modifications

The *reference system* (see Fig. 2.1) has one mixer to blend three flows of different composition: the solution from the degasser has methanol concentrations ranging from 0.1 M to 2 M according to operating conditions, the liquid from the condenser is neat water, and the liquid from the methanol tank is neat methanol. This system is not able to instantaneously adjust the concentration of the solution entering the anode because the large size of the mixer works as a buffer to mitigate concentration changes. In the first modification to the *reference system*, neat methanol is added in an in-line mixer to the flow leaving the mixer tank, as illustrated in Fig. 3.1. In this *two-mixer system*, recycled methanol solution and condensed water are first blended in the large tank mixer; the diluted solution is subsequently concentrated by neat methanol in an in-line mixer with negligible hold up to increase the anode inlet concentration to its optimal value. This feedforward concentration control enables responding promptly to sudden changes in the electric load.

To obtain a further degree of freedom to control concentration, a system with separated solution tanks is also suggested (Fig. 3.2), employing separate reservoirs for spent solution and condensed water. In this layout variation, the methanol concentration can not be only in-

from the *reference system* as listed in Table 3.1. Water drag by electro-osmosis is assumed to be related with current and temperature (T1.3 and T1.4). In this model, as in all other models in this work, the stack is considered as the only equipment with heat capacity.

The heat capacity of the stack C_p^{stack} is estimated to be 3000 J/K for the stack used in experimental validation.

3.2.2 Peripheral devices

Coolers are assumed to be internally cascade-controlled and able to set a given outlet temperature as such in Chapter 2. The degasser and the condenser only separate liquid from gas, which are at perfect equilibrium when leaving the separator (T1.5, T1.6 and T1.7). Energy balance is the summation of each enthalpy of components (T1.8). The methanol loss by evaporation in the degasser of the *reference system* is negligible compared to the electrochemical reaction and crossover, and can also be omitted in this model [37]. The only component which can accumulate materials is the mixer in the system (T1.9). Energy is also dependent on accumulated components (T1.10).

3.2.3 Controller synthesis

In the *reference system*, five decoupled SISO (single-input and single-output) controllers govern the control variable, using each one manipulated variable; as seen in Table 3.2. Of the five controllers in the *reference system*, three controllers for oxygen mole fraction y_{O_2} , condenser temperature T^{cond} and stack temperature T^{stack} will remain unchanged in this chapter, whereas the methanol concentration controller and the controller for anode excess ratio, λ^{an} will be modified for the *two-mixer system* and the *separate-tank system*. In addition, the new degree of freedom introduced by the *separate-tank system*, which has the levels of two tanks instead of a single solution tank, will require an extra controller for retaining solution level.

3.2.3.1 Concentration set-point

The main feature of the two layouts, presented in this chapter, is the ability to change the anodic inlet concentration rapidly; it is, therefore, necessary to present a criterion by which to choose the concentration

Table 3.1: Model equations and parameters valid for *reference, two-mixer and separate-tank system models*

Components	Stack
Component mass balance	$\dot{n}_{j,\text{out}} = \dot{n}_{j,\text{in}} + \nu_j \frac{N \cdot I}{F} + \xi_j \dot{n}_x$ (T1.1)
Energy balance	$C_p^{\text{stack}} \frac{dT^{\text{stack}}}{dt} = \sum_{j,s} h_j (T_{\text{in}}^s) \dot{n}_{j,\text{in}}^s$ $- \sum_{j,s} h_j (T^{\text{stack}}) \dot{n}_{j,\text{out}}^s - UI$ (T1.2)
Electro-osmotic water drag	$\dot{n}_d = N \cdot k_d \frac{I}{F}$ (T1.3)
Electro-osmotic drag coefficient	$k_d = \left(4.2 + \frac{T^{\text{stack}} - 303.15K}{40K} \right)$ (T1.4)
Index	$j : CH_3OH, H_2O, O_2, CO_2, N_2$ $\nu_j^{\text{an}} = \{-1/6, -1/6 - k_d, 0, 1/6, 0\}$ $\nu_j^{\text{cath}} = \{0, 1/2 + k_d, -1/4, 0, 0\}$ $\xi_j^{\text{an}} = \{-1, 0, 0, 0, 0\}$ $\xi_j^{\text{cath}} = \{0, 2, -3/2, 1, 0\}$
Components	Separators
Component mass balance	$\dot{n}_j^{\text{gas}} = \dot{n}_{\text{in},j} \quad j \in \{O_2, CO_2, N_2\}$ (T1.5) $\dot{n}_j^{\text{gas}} = \dot{n}_{\text{in},j} \frac{\beta K_j}{1 + \beta(K_j - 1)}$ $j \in \{CH_3OH, H_2O\}$ (T1.6)
	$\dot{n}_j^{\text{liq}} = \dot{n}_{\text{in},j} - \dot{n}_j^{\text{gas}} \quad \forall j$ (T1.7)
Energy balance	$\dot{h}^{\text{liq}} = \sum_j h_j \times \dot{n}_j^{\text{liq}}$ (T1.8)
Components	Mixer
Component mass balance	$\frac{dn_j^{\text{mix}}}{dt} = \sum_{flows} \dot{n}_{flows,j}$ (T1.9)
Energy balance	$\frac{dE^{\text{mix}}}{dt} = \sum_{flows} \dot{h}_{flows}$ (T1.10)

Table 3.2: Identical controllers for *reference, two-mixer and separate-tank systems*

Controlled Variable	Manipulated Inputs	Disturbance	Measured Outputs	Controller Type
y_{O_2}	\dot{V}_{in}^{cath}	I	I	Feedforward
V^{mix}	\bar{T}^{cond}	T^{cond}, \dot{V}^{cath}	V^{mix}	Feedback
T^{stack}	\bar{T}^{deg}	I, c_{out}^{an}	T^{stack}	P feedback

set-point. The criterion considered in this study is the maximisation of the fuel cells' efficiency η .

There are three components of efficiency to consider:

- Faradaic efficiency φ ,
- Voltage efficiency ε , and
- Thermodynamic efficiency η_{th} .

The product of these is the overall efficiency:

$$\eta = \varphi \varepsilon \eta_{th} \quad (3.1)$$

Faradaic efficiency φ is the ratio of how much methanol is used in the anodic reaction (1.1) out of the total that enters the anodic loop \dot{n}^{fuel} , and at steady state it is expressed by:

$$\varphi = N \frac{I}{6 F} \frac{1}{\dot{n}^{fuel}} \quad (3.2)$$

Voltage efficiency ε is instead the efficiency of the conversion from chemical to electrical energy for the combined reactions (1.1) and (1.2); it can be directly inferred from stack voltage:

$$\varepsilon = \frac{U}{N E^{rev}} \quad (3.3)$$

where $E^{rev} = \Delta g_r / 6 F$ is the reversible cell potential. Finally,

$$\eta_{th} = \frac{\Delta g_r}{\Delta h_r} \quad (3.4)$$

where Δh_r is the enthalpy of the total reaction from reactions (1.1) and (1.2).

This study will focus on faradaic efficiency φ , since it is the most amenable to study with a system model and controllers directly with fuel loss. The voltage efficiency ε has been previously studied [38], establishing that there is an optimal concentration at which voltage is maximum: higher concentrations promote more crossover (increasing the cathodic overvoltage), and lower concentrations increase anodic overvoltage because of reactant starvation.

Neglecting losses in the degasser, which are relatively small [1], the faradaic efficiency can be approximated with the ratio of methanol consumed in the anodic reaction (1.1) to all the methanol reacted in the fuel cell, including crossover:

$$\tilde{\varphi} \approx \frac{I/6F}{I/6F + \dot{n}_x/N} \quad (3.5)$$

Inserting yields the expression for crossover flow in Equation 2.13 and solving for anodic concentration yields:

$$\bar{c}_{\text{out}}^{\text{an}} = \frac{I}{6F} \left(\frac{1}{\tilde{\varphi}} + \tilde{b} - 1 \right) \frac{1}{\tilde{a}A} \quad (3.6)$$

where $\tilde{\varphi}$ is the target faradaic efficiency, and \tilde{a} and \tilde{b} are estimates of the crossover parameters.

It is not realistic to simply set the target to $\tilde{\varphi} = 1$, which would imply no crossover: this would mean that the methanol concentration at the anodic catalyst layer would be zero, which would result in reactant starvation and high anodic overvoltage: $\varphi \rightarrow 1$ implies $\varepsilon \rightarrow 0$, bringing total efficiency η also to zero.

An exact target faradaic efficiency can be obtained optimising η , which in general requires a detailed electrochemical model to calculate ε as a function of current and methanol concentration; for simplicity, in this study, a constant target of $\tilde{\varphi} = 65\%$ is assumed to prevent experimentally-observed fuel deficiency at the anode catalyst layer due to low inlet concentration. The anode outlet concentration, which is the one that determines crossover in our model, is approximated with relation to λ^{an} and inlet concentration $\bar{c}_{\text{in}}^{\text{an}}$ in the following way:

$$(\lambda^{\text{an}} - 1)\bar{c}_{\text{in}}^{\text{an}} \approx \lambda^{\text{an}}\bar{c}_{\text{out}}^{\text{an}} \quad (3.7)$$

Combining Equations (3.6) and (3.7) yields:

$$\bar{c}_{in}^{an} = \frac{I}{6F} \left(\frac{1}{\tilde{\varphi}} + \tilde{b} - 1 \right) \frac{1}{\tilde{a} A} \frac{\lambda^{an}}{\lambda^{an} - 1} \quad (3.8)$$

3.2.3.2 Concentration estimate

In the two newly proposed layouts, it is necessary to have an estimate of the concentration in the mixer \tilde{c}^{mix} or solution tank \tilde{c}^{sol} where it is stored. Concentrations are calculated by the estimated amount of methanol $\tilde{n}_{CH_3OH}^{mix}$ or $\tilde{n}_{CH_3OH}^{sol}$ and by a measured or estimated solution volume V^{mix} :

$$\tilde{c}^{mix} = \frac{\tilde{n}_{CH_3OH}^{mix}}{V^{mix}} \quad \text{for the } two\text{-mixer system} \quad (3.9)$$

$$\tilde{c}^{sol} = \frac{\tilde{n}_{CH_3OH}^{sol}}{V^{sol}} \quad \text{for the } separate\text{-tank system} \quad (3.10)$$

In turn, the amount of methanol in the mixer or solution tank $n_{CH_3OH}^{mix/sol}$ is estimated by integrating the estimated rate of methanol accumulation from fuel supply and consumption from the reactions:

$$\frac{d \tilde{n}_{CH_3OH}^{mix/sol}}{dt} = \frac{\rho_{CH_3OH}}{M_{CH_3OH}} \dot{V}^{fuel} - N \left[\frac{I}{6F} (1 - \tilde{b}) + \tilde{a} A \tilde{c}_{out}^{an} \right] \quad (3.11)$$

where the estimated crossover parameters \tilde{a} and \tilde{b} are experimentally determined at 60 °C.

3.2.3.3 Two-mixer system

This system has a single solution tank where both the degasser effluent and recovered water are mixed. Compared to the *reference system*'s controllers summarised in Table 3.2, the *two-mixer system* has a completely different dynamic controller for concentration, and a slightly different implementation for the constant λ control on the anodic side.

Both anodic λ^{an} and inlet concentration are influenced by the fuel pump and the circulation pump as seen in Fig. 3.3, so the controller is chosen to be a 2×2 MIMO (multi-input, multi-output) feedforward controller.

The controller includes an estimator for methanol concentration in the mixer, implemented as in Equation (3.11); \tilde{c}^{mix} is therefore assumed known in the following. It is also assumed that the set-point for inlet concentration $\bar{c}_{\text{in}}^{\text{an}}$ is known from Equation (3.8).

Two equations must be solved simultaneously to determine \dot{V}^{fuel} and \dot{V}^{sol} for λ^{an} and inlet concentration control.

The condition for constant λ control is that the total inflow of methanol into the stack is λ times the methanol consumption in the stack due to the anodic reaction and crossover:

$$\bar{c}_{\text{in}}^{\text{an}} (\dot{V}^{\text{fuel}} + \dot{V}^{\text{sol}}) = \lambda^{\text{an}} N \left[\frac{I}{6F} (1 - \tilde{b}) + \tilde{a} A \tilde{c}^{\text{mix}} \right] \quad (3.12)$$

The condition for concentration control depends on whether the estimated concentration in the mixer tank, \tilde{c}^{mix} , is higher or lower than the set-point $\bar{c}_{\text{in}}^{\text{an}}$: if \tilde{c}^{mix} is higher, the fuel flow will be set to zero, since negative values are not possible. The condition is expressed as the methanol balance around the in-line mixer:

$$\begin{cases} \bar{c}_{\text{in}}^{\text{an}} (\dot{V}^{\text{fuel}} + \dot{V}^{\text{sol}}) = \frac{\rho_{\text{CH}_3\text{OH}}}{M_{\text{CH}_3\text{OH}}} \dot{V}^{\text{fuel}} + \tilde{c}^{\text{mix}} \dot{V}^{\text{sol}} & \text{if } \tilde{c}^{\text{mix}} < \bar{c}_{\text{in}}^{\text{an}} \\ \dot{V}^{\text{fuel}} = 0 & \text{otherwise} \end{cases} \quad (3.13)$$

The values of the manipulable variables \dot{V}^{fuel} and \dot{V}^{sol} can be found by solving the linear algebraic Equations (3.12) and (3.13).

3.2.3.4 Separate-tank system

In the *separate-tank system*, the condensed water in the condenser gathers in its own tank instead of being mixed with the recycled solution from the stack. This allows to blend the solution from the solution tank with water in order to produce an anode inlet concentration lower than the one in the solution tank: this can be useful to reduce crossover after a sudden reduction in power output. The *separate-tank system* contains the additional complexity of controlling the liquid level in an additional tank, but the control rules are inspired by the same principles as for the *reference system*. The previous feedback level controller for the mixer in Chapter 2 is applied, unchanged, to one tank (water tank); it is therefore the other tank (solution tank) that will need a new controller (MIMO controller).

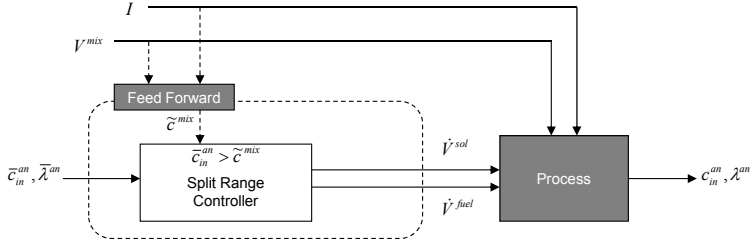


Fig. 3.3: The block diagram of the MIMO feedforward concentration and λ controller in the *two-mixer system*.

The three manipulated variables are the flows of neat methanol, solution and water: \dot{V}^{fuel} , \dot{V}^{sol} , and \dot{V}^{water} . The three control objectives are constant λ^{an} control, controlling $c_{\text{in}}^{\text{an}}$, and maintaining the level of the solution tank. All three control variables are influenced by all three manipulated inputs, and therefore, a 3×3 MIMO controller is chosen.

As for the case of the *two-mixer system*, the controller for the *separate-tank system* includes a concentration estimator (for the solution tank) and assumes that the reference inlet concentration $\bar{c}_{\text{in}}^{\text{an}}$ is given as in Equation 3.8.

The control equations for λ^{an} and concentration control are structurally similar to the case of the *two-mixer system*. For λ control it is:

$$\bar{c}_{\text{in}}^{\text{an}} (\dot{V}^{\text{fuel}} + \dot{V}^{\text{sol}} + \dot{V}^{\text{water}}) = \lambda^{\text{an}} N \left[\frac{I}{6F} (1 - \tilde{b}) + \tilde{a} A \tilde{c}^{\text{sol}} \right] \quad (3.14)$$

For concentration control it is:

$$\bar{c}_{\text{in}}^{\text{an}} (\dot{V}_c^{\text{fuel}} + \dot{V}_c^{\text{sol}} + \dot{V}_c^{\text{water}}) = \frac{\rho_{\text{CH}_3\text{OH}}}{M_{\text{CH}_3\text{OH}}} \dot{V}_c^{\text{fuel}} + \tilde{c}^{\text{sol}} \dot{V}^{\text{sol}} \quad (3.15)$$

In an extension of the condition given in Equation (3.13), either water or fuel flow is stopped depending on the estimated concentration in the

solution tank:

$$\begin{cases} \dot{V}_c^{\text{water}} = 0 & \text{if } \bar{c}^{\text{sol}} < \bar{c}_{\text{in}}^{\text{an}} \\ \dot{V}_c^{\text{fuel}} = 0 & \text{otherwise} \end{cases} \quad (3.16)$$

In both Equations (3.15) and (3.16), a subscript c has been added to water and fuel flows, to indicate these are components of the flows that are used to control concentration. Water and fuel flows are also used to control the solution tank's level, and those components are indicated with the subscript v and explained in the following.

The dynamics of solution volume is an integrator of the volumetric water and fuel flows, which means that it requires feedback to be stabilised; it is assumed that a measurement or estimate \tilde{V}^{sol} of the solution tank volume is available.

The liquid volume in the solution tank is controlled with a proportional feedback controller (P controller), integrated into the 3×3 MIMO controller. The controller attempts to maintain a set-point volume \bar{V}^{sol} by manipulating water and fuel flows. A simple P controller can be set up as follows [36]:

$$\dot{V}_V^{\text{fuel}} + \dot{V}_V^{\text{water}} = \begin{cases} \frac{1}{\tau_c} (\bar{V}^{\text{sol}} - \tilde{V}^{\text{sol}}) & \text{if } \tilde{V}^{\text{sol}} < \bar{V}^{\text{sol}} \\ 0 & \text{otherwise} \end{cases} \quad (3.17)$$

Note that, if the actual volume in the solution tank is larger than the set-point, flow \dot{V}_V^{fuel} and \dot{V}_V^{water} are set to zero since they cannot be negative; over time, the volume of the solution loop will decrease due to electro-osmotic drag in the stack. Constant τ_c is a design parameter corresponding to the desired response time of the controlled process; since the open-loop dynamics of the process is fast, it can be set to a low value, e.g. 60 s.

Finally, the fuel and water flows will need to be dosed according to Equation 3.18, so that the solution volume controller does not interfere with concentration control to the set value $\bar{c}_{\text{in}}^{\text{an}}$:

$$\bar{c}_{\text{in}}^{\text{an}} (\dot{V}_V^{\text{fuel}} + \dot{V}_V^{\text{water}}) = \frac{\rho_{\text{CH}_3\text{OH}}}{M_{\text{CH}_3\text{OH}}} \dot{V}_V^{\text{fuel}} \quad (3.18)$$

The concentration to the anodic inlet can obviously be increased only by the fuel flow rate.

The actual fuel and water flows set by the pumps in Fig. 3.4 are the

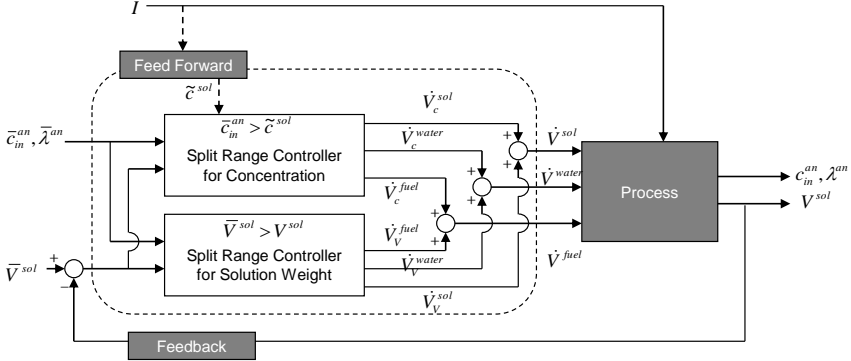


Fig. 3.4: The block diagram of the concentration and volume controller in the *separate-tank system*.

sums of volume-control and concentration-control flow components:

$$\dot{V}^{\text{fuel}} = \dot{V}_V^{\text{fuel}} + \dot{V}_c^{\text{fuel}} \quad (3.19)$$

$$\dot{V}^{\text{water}} = \dot{V}_V^{\text{water}} + \dot{V}_c^{\text{water}} \quad (3.20)$$

Virtually splitting the flows in these components is the most straightforward way to enforce the constraint that flows need to be larger than zero across several parts of the MIMO controller.

3.3 Experimental set-up

The layout of the *reference system* in Chapter 2 is modified to the *two-mixer system* and the *separate-tank system*, sequentially. The *two-mixer system* is equipped with the in-line static mixer (Plastic Static Mixer 103201, ESSKA.de GmbH, Germany) with 10mm of inner diameter and 100mm of length in between pumps and the anode inlet. Except for the static mixer, the other components and measuring devices are the same as for the *reference system*. The layout of the *separate-tank system* has no tank mixer anymore. It instead employs two container tanks for storing water and methanol solution from condenser and degasser, respectively. Both the *two-mixer system* and the *separate-tank system* are implemented with the controllers presented in Section 3.2.3. Operating procedure is identical to that of the *reference system* exper-

Table 3.3: Absolute root mean square error between experiment and simulation of each system for stack temperature, inlet and outlet concentration

	Two-mixer	Separate-tank
Stack Temperature /°C	7.85 (Fig.3.6a)	5.64 (Fig.3.6b)
Inlet Concentration /M	0.266 (Fig.3.7a)	0.263 (Fig.3.7c)
Outlet Concentration /M	0.203 (Fig.3.7b)	0.175 (Fig.3.7d)

iment in Chapter 2 including preconditioning and current disturbance as shown in Fig. 2.10.

3.4 Results and discussion

To compare the various systems under dynamic operation, the same current profile is applied to all systems as shown in Fig. 2.10. The simulated voltage response for all three systems is identical because the voltage is calculated by the Thévenin equivalent circuit and assumed to be independent from temperature and concentration. The Thévenin parameters correspond to a set temperature of 60 °C and set concentration of 1000 mol/m³. The results are expected to deviate from the experiments where this dependence will not be negligible. At start-up, the experimental voltages of all three systems are lower than in the simulation as is visible in Fig. 3.5, which is attributed to the experimental stack temperature being lower than the set temperature, as observed in Fig. 3.6. After the start-up period, *reference system* fits the voltage response of Thévenin equivalent circuit because the stack temperature in the *reference system* remained at 60 °C. However, the newly presented systems in this chapter - *two-mixer system* and *separate-tank system* - showed much lower stack temperature than the *reference system* in the whole period except for the stack temperature in *separate-tank system* at the first one-hour period. In that period, the stack temperature in *separate-tank system* reaches set temperature owing to the overshoot of the concentration control. In Table 3.3, root mean square errors are listed for the quantitative comparison of the simulation and experimental results. The error between experiment and simulation of

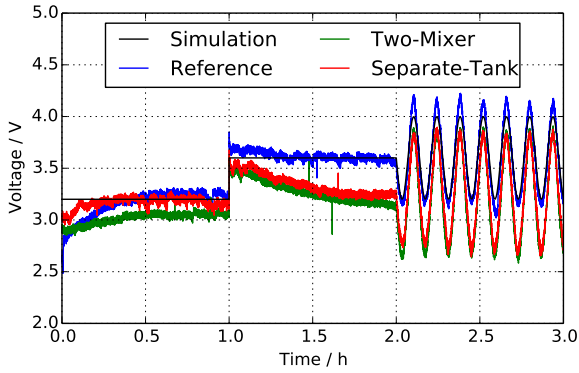
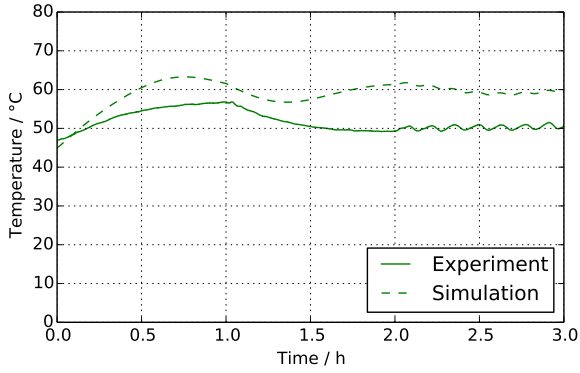
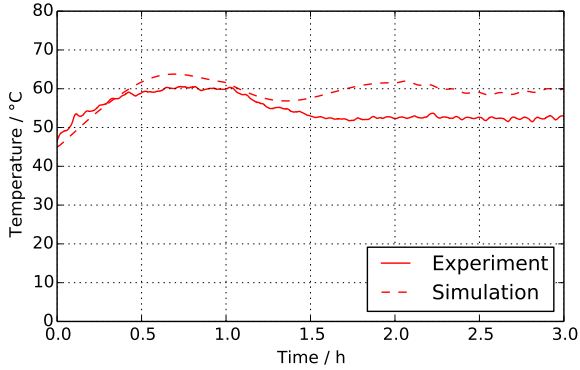


Fig. 3.5: the resulting output voltage in simulations and experiments for all systems.

separate-tank system for stack temperature is smaller than that of *two-mixer system*. Each value is discussed at related sections further on.



(a)



(b)

Fig. 3.6: The temperature profile of the stack in (a) *two-mixer system* and (b) *separate-tank system*

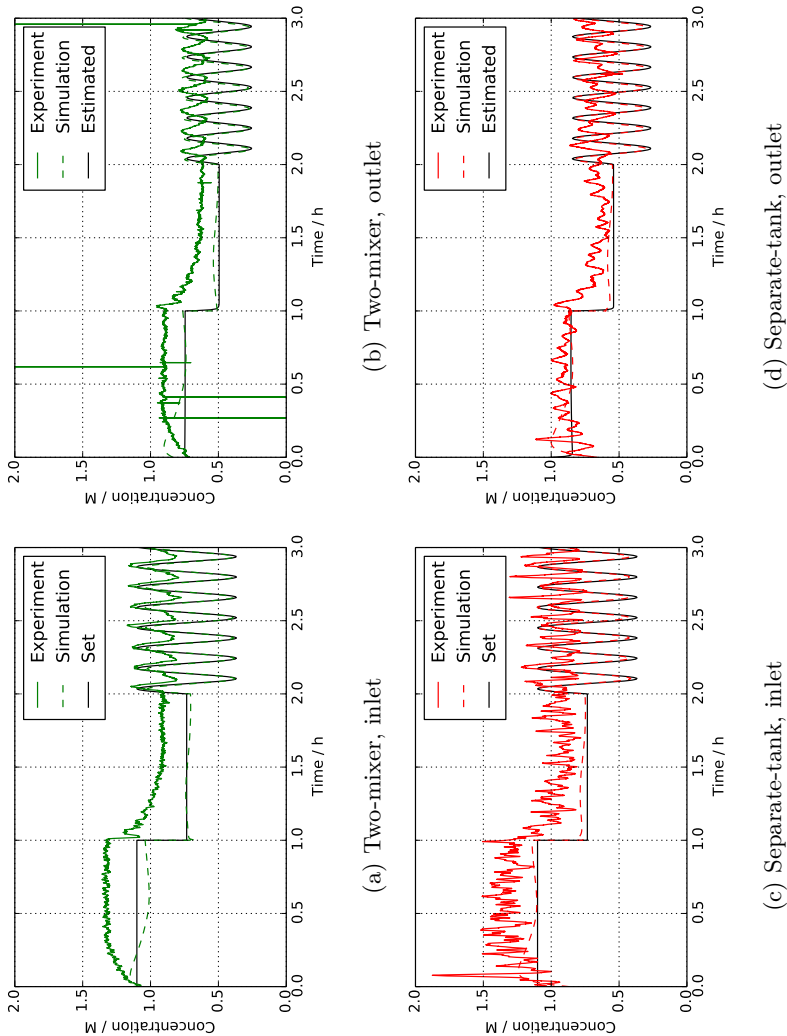


Fig. 3.7: Stack inlet and outlet concentrations for all systems (Estimated values are calculated identically in both simulation and experiment)

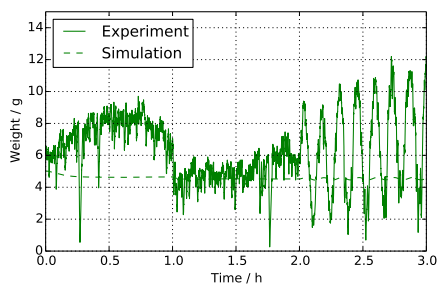
3.4.1 Two-mixer system

The experimental stack temperature of the *two-mixer system* cannot reach 60 °C during the whole period, as can be seen in Fig. 3.6a and Table 3.3. The experimentally-observed low temperature of the stack results from the heat loss from the stack surface, which was not considered in the model. The heat loss is not significant in the *reference system*, because excessive heat is generated by the large amount of methanol oxidation of the methanol crossover, which is minimized in the *two-mixer system* to achieve high faradaic efficiency. Due to the low stack temperature in the experiment, methanol crossover occurs less than in the simulation [32]. However, the fuel flow controller, which is only calibrated at 60 °C with parameters a and b , supplies more methanol to the system than the estimated amount in the simulation, as shown in Fig. 3.7a and 3.7b. In real systems, therefore, either a and b need to be given as temperature dependent.

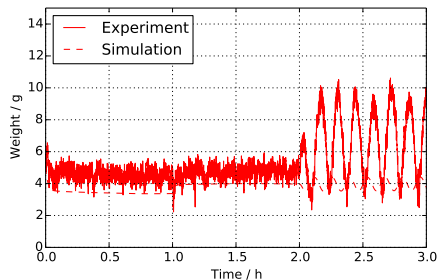
3.4.2 Separate-tank system

The solution volume in the solution tank of the *separate-tank system* is lower than the set value 5 ml owing to the volumetric offset of the P controller (Fig. 3.8b). According to Equation 3.10 the solution volume V^{sol} , the water flow rate \dot{V}_V^{water} and the fuel flow rate \dot{V}_V^{fuel} are positive. This abundant fuel flow \dot{V}_V^{fuel} for the volume control, besides the fuel flow \dot{V}_c^{fuel} for the concentration control, makes the summated flow rate \dot{V}^{fuel} larger than that in the *two-mixer system*. The excessive fuel flow in the *separate-tank system* heats up the stack to higher temperature than that in the *two-mixer system*, as shown in Fig. 3.6b and Table 3.3. In the *separate-tank system*, the concentration profiles of the experimental results (Fig. 3.7c and 3.7d) are closer to those of the simulation results than those in the *two-mixer system* in Table 3.3, because in the *separate-tank system*, the outlet concentration is more precisely estimated using the additional water flow rate \dot{V}^{water} than that in the *two-mixer system*. The mixture of water and neat methanol can be accurately calculated when each flow rate is known.

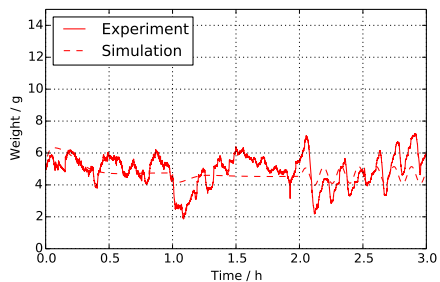
The high-frequency noise in the concentration, visible in the *separate-tank system*, is due to the volume controller for the solution tank: the strain gauge for the solution weight measurement is sensitive to the presence of liquid droplets from the condenser and the degasser, which induce noisy sensor readings and an equally noisy control action. This



(a) Two-mixer



(b) Separate-tank, solution



(c) Separate-tank, water

Fig. 3.8: (a) Solution weight measurement of the tank mixer in the *two-mixer system*, (b) solution weight of the solution tank and (c) water weight of the water tank in the *separate-tank system*, respectively

noise may be easily removed with a low-pass filter in a further refinement of the control system.

3.4.3 Faradaic efficiencies

As shown in Fig. 3.9a, the efficiency of the *two-mixer system* is marginally higher than that of the *separate-tank system*, while both are significantly higher than the *reference system* (Fig. 2.15, especially at low currents. This is due to the higher concentration maintained by the *reference system*, which results in higher crossover and reduced efficiency. The simulations are validated by experimental results, as shown in Fig. 3.9b. The noise for the experimental results of the *separate-tank system* is due to the noisy weight measurement and peristaltic pumping, as explained above.

The difference between *two-mixer* and *separate-tank system* is attributed to the supplied fuel flow (\dot{V}_V^{fuel}) for volume control which is consumed and lowers the faradaic efficiency below the set value 65 % in Section 3.2.3.1.

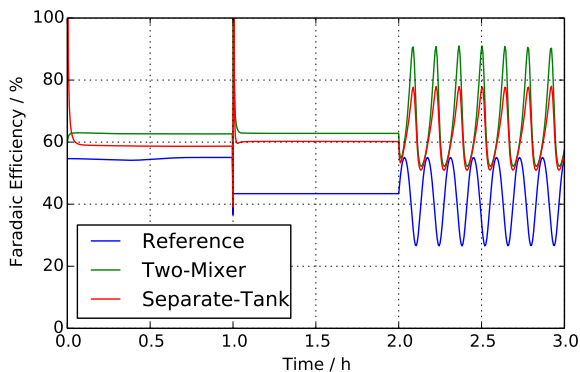
3.4.4 Liquid holdup in solution tanks

The solution weight control was able to stabilise the amount of solution and water level (*separate-tank system* only) for all system designs and operating conditions; however, the measured weights fluctuated strongly in experiments, as shown in Fig. 3.8.

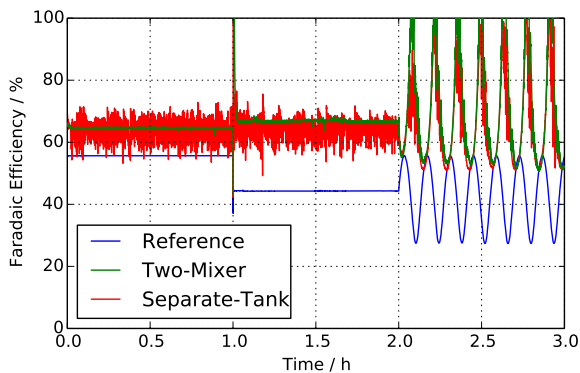
This is due to the aforementioned sensitivity of the strain gauge to discontinuous two-phase flow: the carbon dioxide produced by the anodic reaction (1.1) leaves discontinuously the degasser and leads to the noisy measurements seen in Fig. 2.16, Fig. 3.8a and Fig. 3.8b, while the water tank is independent from the degasser and the corresponding weight fluctuates less, as seen in Fig. 3.8c.

The rising solution weight at the beginning in Fig. 3.8a is attributed to the initially low stack temperature, which allows more water to condense than expected at the controller who assume a value of 60 °C.

In the last hour of experiments, the weight of the solution tanks oscillate much more than predicted by simulations; these oscillations are in phase with the current's. This increased amplitude is due to the effect of varying gas fraction in the stack's anode channels and the tube leading from the anode outlet to the degasser, since CO₂ production on the anodes, is proportional to current according to Reaction (1.1):



(a) Simulations



(b) Experiments

Fig. 3.9: Faradaic Efficiencies of the various systems in simulations and experiments.

as current increases, more gas is present in the channels and liquid is displaced to the solution tanks. This effect is not present in simulations since the model neglects hold-up in the stack and tubes, which is considered in the next chapter.

3.5 Conclusions

Using a dynamically set inlet concentration in DMFC systems instead of a constant concentration has been demonstrated to significantly improve faradaic efficiency under variable load conditions in simulation and experiments.

Both proposed layouts, *two-mixer system* and *separate-tank system*, have experimentally similar time constants for transients in concentration control, which are larger than those in simulations. The *separate-tank system* is able to follow the set concentration with slightly better precision, since part of the anode inlet flow is blended from two reservoirs of known concentration (fuel and water).

In experiments, the *separate-tank system* has been shown to be subject to oscillations in anode inlet concentration originating from sensor noise propagating through a P controller; a low-pass filter should, however, be sufficient to ameliorate the issue in a further development.

All experimental systems present significant oscillations in liquid holdup under variable current conditions compared to simulations, due to different rates of CO_2 production in the anode and consequent liquid displacement by gas.

In experiments, the reduced crossover resulted in less heat generation, so that the stack could not reach the set-point temperature of 60°C in either of the new proposed systems; as a result, the crossover was further reduced by the lower temperature, and the measured concentrations were higher than in simulations. The low temperature also resulted in lower voltage than the simulation.

Heat loss from large exposed areas in a laboratory setup also cooled down the stack in addition, which should not be an issue in mass-produced, integrated systems.

The *two-mixer system* is, in general, preferable, in particular for portable applications, as it comprises fewer components while featuring essentially the same advantages as the *separate-tank system*.

Simplifying the *two-mixer system* with process integration is designed and investigated in the next chapter. On top of that, the stack model

including material hold-up, which was not considered in this chapter, is introduced and examined for the accurate controllers in Chapter 4.

Chapter 4

System variation for process integration³

In this research, DMFC systems are considered as portable power sources for small electric devices such as laptops, which widely use Li-ion batteries. If DMFC systems are as small as batteries, DMFC systems can be competitive with batteries because methanol has more energy density than lithium as a fuel [22]. However, typical DMFC systems need several pumps, separators or mixers to operate autonomously using neat methanol. The hydraulic components require relatively large space - often much larger than fuel volume itself [39]. To compete with batteries, DMFC systems should be smaller than current systems. Minimising component size has limitations to physically necessary volumes to exert their own functions. The other way to reduce the system size is combining components and integrating processes. Na *et al.* [40] reduced the number of components with time sharing pumping method so that one pump is used to supply either methanol solution or neat methanol, at a certain point in time. The sharing time depends on methanol concentration in the mixer, therefore a methanol concentration sensor is necessary. Without a concentration sensor, Zenith *et al.* [37] simulated a *mingled-outlet system*, which had reduced components compared to the *reference system* [1]. Two components were able to be removed by process integration of cathode and anode outlet. However, the *mingled-outlet system* has lower fuel efficiency than the *reference system* due to a large amount of methanol evaporation at the mingled outlet.

³Part of the results of this chapter was published in Federico Zenith, Youngseung Na and Ulrike Krewer, *Chemical Engineering and Processing: Process Intensification*, 59: 43–51, 2012.

In this chapter, modelling of the *mingled-outlet system* is validated with experiments, and assumptions in the model are refined to get more realistic results. Then a further system, *highly-integrated system* is introduced and compared with the previous systems.

4.1 System modifications

The *reference system* in Fig. 2.1 was previously analysed in the literature; the present chapter proposes instead lighter, simpler systems which integrate processes and combine outlet coolers and separators. The *reference system* has two coolers and two separators - degasser and condenser - placed at anode and cathode outlet. The coolers have the same function of cooling down two phase flow even if the ratio of gas and liquid is quite different from each other. For process integration, fuel cell's anodic and cathodic product streams are mixed before being sent to a cooler and then to a separator as illustrated in Fig. 4.1 [37]. An even further integrated system is also introduced in this chapter, named *highly-integrated system*. It combines the separator and the mixer to one device as shown in Fig. 4.2. To prevent the evaporation of neat methanol in the separator, fuel is supplied after the separator and mixed in the tube with a static mixer.

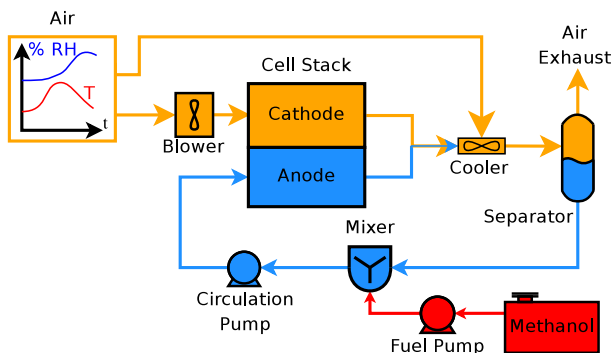


Fig. 4.1: The process scheme of the *mingled-outlet system* [37]

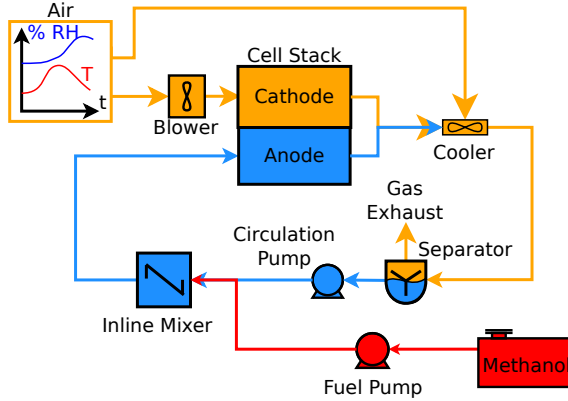


Fig. 4.2: The process scheme of the *highly-integrated system*

4.2 Modelling

The model of the *mingled-outlet system* from the research of Zenith *et al.* [37] is updated with a liquid hold up at the anode channel in the stack, while in the previous model, liquid solution was assumed to accumulate only in the mixer. The larger stack is employed in this study to investigate responses of fuel cell systems at the actual power ranges in several dozen watts. To implement the modified assumption into the model, liquid and gas equilibrates in the anode channels of the stack. The *highly-integrated system* inherited the base model from the *mingled-outlet system* except for the separator. The separator in the *highly-integrated system* has the additional feature of material holdup as a buffer, which was the function of the mixer in the *mingled-outlet system*. The controlling strategy of the system is combined with the dynamic concentration control scheme of the *two mixer system* in Chapter 3 and the stack temperature controller from the *mingled-outlet system*. The respective model modifications are presented in the following.

4.2.1 Fuel cell

To implement material hold up in the anode channel of the stack, the reaction and accumulation process are virtually separated.

Firstly, the species mass balances including anodic reaction 1.1 are identical to that of the *reference system* in Table 3.1. After reaction, the resulting anode product stream equilibrates according to Rachford-Rice Equations 2.5, 2.6 of stack operating conditions such as temperature and pressure in Section 2.1.1. Equilibrated products $\dot{n}_{out,j}$ are accumulated in virtual reservoir with the volume of V^{holdup} .

Secondly, the gaseous carbon dioxide generated by the anodic reaction 1.1 has a very low density, and displaces liquid from the anode channels through the stack outlet; this can have significant effects when current is rapidly changed. For instance, when no electric load is drawn, the anodic channel is full of liquid solution. If current is drawn, carbon dioxide is produced and pushes out some amount of liquid solution to the outlet by following equation:

$$V^{\text{holdup}} = V^{\text{gas,holdup}} + V^{\text{liq,holdup}} \quad (4.1)$$

The sum of volume of liquid and gas is limited to the total volume V^{holdup} of the anode channel. The material holdup reservoir is calculated as a virtually separated volume V^{holdup} without electrochemical reactions, which are already calculated in the stack, for avoiding interference to the anodic reaction. Material and energy balance of each species in each phase in the material holdup reservoir are calculated as follows:

$$\frac{dn_j^{\text{holdup}}}{dt} = \dot{n}_{in,j}^{\text{holdup}} - \dot{n}_{out,j}^{\text{holdup}} \quad (4.2)$$

$$\frac{dE^{\text{holdup}}}{dt} = \dot{H}_{in,j}^{\text{holdup}} - \dot{H}_{out,j}^{\text{holdup}} \quad (4.3)$$

The expelled two phase flow passes through the cooler and the separator in turn.

4.2.2 Cooler

The cooler model is identical to that of the *reference system* in Chapter 2. It merges methanol, water and carbon dioxide from anode outlet with water, oxygen and nitrogen from cathode outlet. Outlet temperature follows set temperature as first order time lag, see Equation 2.19.

4.2.3 Integrated separator

The integrated separator splits gas and liquid flows from the sum of cathode and anode outlets, like the separator in the *mingled-outlet system*. Incondensable components leave the separator from the gas outlet only as given in Equation 4.4, whereas methanol and water leave from both liquid and gas outlets; the gas-liquid equilibrium is solved through Equation 4.5 and 4.6.

$$\dot{n}_{\text{gas},j} = \dot{n}_{\text{in},j} \quad j \in \{O_2, CO_2, N_2\} \quad (4.4)$$

$$\dot{n}_{\text{gas},j} = \dot{n}_{\text{in},j} \frac{\beta K_j}{1 + \beta(K_j - 1)} \quad j \in \{CH_3OH, H_2O\} \quad (4.5)$$

$$\dot{n}_{\text{liq},j} = \dot{n}_{\text{in},j} - \dot{n}_{\text{gas},j} \quad j \in \{CH_3OH, H_2O\} \quad (4.6)$$

The function of material holdup like the mixer of the *reference system* is added to the integrated separator as follows:

$$\frac{dn_j^{\text{sep}}}{dt} = \sum_{\text{flows}} \dot{n}_{j,\text{flows}} \quad j \in \{CH_3OH, H_2O\} \quad (4.7)$$

Subscript *flows* indicates inlet flow into the integrated separator from the cooler, gas outlet flow to the atmosphere or liquid outlet flow into the circulation pump as described in Fig. 4.2. Energy balance is calculated based on the summation of each enthalpy as follows:

$$\frac{dE^{\text{sep}}}{dt} = \sum_{\text{flows}} \dot{h}_{j,\text{flows}} \quad j \in \{CH_3OH, H_2O\} \quad (4.8)$$

4.2.4 Controller synthesis of mingled outlet system

4.2.4.1 Solution-Volume Control

Since the anodic methanol solution is very diluted, controlling solution volume is equivalent to controlling the amount of water in the system.

In the context of DMFC systems, autonomy has been defined as the ability of the system to maintain a constant water content in its anodic loop, without an external supply or sink. It was previously shown in Chapter 2 that the *reference system*'s water balance produces a relationship binding only three variables: environmental humidity, cathodic air excess ratio and condenser temperature⁴. This means that, given the environmental conditions and the air excess ratio, there is one condenser temperature that guarantees system autonomy; in particular, no cell variables or parameters are relevant to autonomy [11].

The theory developed for the *reference system* stems from a system-wide water balance, so it can be immediately extended to the *mingled-outlet system* in Fig. 4.1 since the total flow of exhaust gases is the same.

The water-content control developed for the *reference system* (a P controller with gain scheduling) as introduced in section 2.1.6.2 can, therefore, be used in the *mingled-outlet system*, with no modification other than it is now applied to the common separator temperature.

4.2.4.2 Temperature control

In the *reference system*, control of stack temperature is realised by manipulation of the degasser temperature, which in turn can be realised through manipulation of the air flow rate in the cooler as discussed in Section 2.1.6.3. However, that degree of freedom is lost in the integrated design, as the single separator's temperature needs to be assigned to the solution-volume control. A different approach to control stack temperature is therefore employed.

The methanol solution flow (Equation 2.31), which in the *reference system* is simply set to maintain a specific anodic excess ratio λ^{an} , shall

⁴Strictly speaking, the relationship holds exactly only when the anodic and cathodic cooling temperatures are equal, but deviations were proven to have only a minor effect. In any case, the condition does hold for the integrated system.

be used to control stack temperature. Effectively, this amounts to using the loop solution as a cooling liquid.

The many uncertainties about heat loss terms in the system, and the ease with which temperature can be measured, suggest using feedback control. Also, stack temperature has a strong effect on several system parameters, in particular anode kinetics and cross-over in the fuel cells: therefore, the control algorithm should have no steady-state offset. A proportional-integral (PI) feedback controller satisfies these requirements, and will be used to control the stack temperature by manipulating the solution flow.

The PI controller is synthesised according to the Skogestad rules [36]. For that purpose, a simple model of the process between manipulated and control variables, i.e. between solution flow and stack temperature, is necessary. Stack temperature is indeed influenced by several other variables that may have an even stronger influence than solution flow: these are considered disturbances as solution flow cannot influence them, and will have to compensate for their variations. The dynamics of stack temperature is given by the stack's energy balance:

$$C_p^{\text{stack}} \frac{dT^{\text{stack}}}{dt} = - \overbrace{c_{p,\text{H}_2\text{O}} (T^{\text{stack}} - T^{\text{mix}}) \dot{V}^{\text{an}}}^{\text{Cooling by anodic solution}} + d \quad (4.9)$$

where d is the disturbance term, and includes the effects of air flow, the heat of reaction, heat loss from the stack, temperature of inlet flows, etc. This dynamic equation is nonlinear in the term $T^{\text{stack}} \dot{V}^{\text{an}}$, which is the product of the control variable (T^{stack}) and the manipulated variable (\dot{V}^{an}). Given the prevalence of water in the methanol solution (95%_{mass}), water's specific heat capacity has been used directly.

To linearise the problem, it will be assumed that the temperature difference across the stack in the anodic flow, $\Delta T \triangleq T^{\text{stack}} - T^{\text{mix}}$, is measured by a thermocouple and can be used as an input in the control algorithm.

This approach does introduce a hidden feedback in the controller which may cause instability, but it also greatly simplifies controller design: the transfer function between \dot{V}^{an} and T^{stack} is now an integrating process:

$$G(s) = - \frac{c_{p,\text{H}_2\text{O}} \Delta T}{C_p^{\text{stack}} s} \quad (4.10)$$

For such a process, Skogestad's rules produce a PI controller with gain K_c and integrating time τ_I given by:

$$K_c = -\frac{C_p^{\text{stack}}}{\tau_c \Delta T c_{p,\text{H}_2\text{O}}} \quad (4.11)$$

$$\tau_I = 4 \tau_c \quad (4.12)$$

where τ_c is the desired closed-loop time constant, which is set to 20 s.

The volumetric flow required by the PI controller will then be:

$$\dot{V}_{PI}^{\text{an}} = K_c (\bar{T}^{\text{stack}} - T^{\text{stack}}) + \int \sigma \frac{K_c}{\tau_I} (\bar{T}^{\text{stack}} - T^{\text{stack}}) dt \quad (4.13)$$

While manipulating the anodic flow to control stack temperature, it is simultaneously important to ensure a sufficient inflow of methanol into the stack. A minimum anodic inlet flow is derived from Equation 2.31:

$$\dot{V}_\lambda^{\text{an}} = \lambda_{\min}^{\text{an}} \frac{N}{\dot{c}_{\text{mix}}} \overbrace{\left[\tilde{a} A \dot{c}_{\text{out}}^{\text{an}} + (1 - \tilde{b}) \frac{I}{6 F} \right]}^{\text{Methanol consumption}} \quad (4.14)$$

Methanol concentration $\dot{c}_{\text{out}}^{\text{an}}$ is assumed to be set by the concentration control loop, typically to 1 M, and known with a good approximation during operation. \tilde{c}^{mix} is the minimally estimated concentration in the mixer to avoid fuel starvation in anode. The minimum excess ratio $\lambda_{\min}^{\text{an}}$ is set for the scope of this research to 2.

Especially when stack temperature is lower than the set temperature, PI controlled anodic flow \dot{V}_{PI}^{an} tends to be zero or beneath to heat up the stack without heat loss of solution flow. Therefore, the requirement of minimum anodic λ is then enforced by selecting the highest value between $\dot{V}_\lambda^{\text{an}}$ and \dot{V}_{PI}^{an} :

$$\dot{V}^{\text{an}} = \max(\dot{V}_\lambda^{\text{an}}, \dot{V}_{PI}^{\text{an}}) \quad (4.15)$$

As this approach could cause significant wind-up phenomena in the PI controller when it is operated for a long time by the constant λ control (for example at start-up), the PI controller implements conditional

integration:

$$\sigma = \begin{cases} 0 & \dot{V}_\lambda^{\text{an}} > \dot{V}_{PI}^{\text{an}} \\ 1 & \text{otherwise} \end{cases} \quad (4.16)$$

4.2.4.3 Concentration control

The methanol concentration in the *reference system* was controlled by feedforward, which was possible because of the stable dynamics of concentration and the possibility of estimating the cross-over flux.

In the *mingled-outlet system*, the dynamics of methanol concentration is still stable, but there is an additional non-negligible methanol loss term in the anodic loop that has to be accounted for: the loss of methanol vapour from the single separator. Some loss of methanol vapour also occurs in the *reference system*, but the small gas flow from the degasser makes the loss negligible [1]. In the integrated system, the anodic solution is brought into contact with a much larger gas flow, which allows much more methanol to escape. For feedforward control to work, this loss has to be estimated.

The methanol loss through contact of a water-methanol solution with an unspecified flow \dot{n}_{dry} of incondensable gases is:

$$\dot{n}_{\text{CH}_3\text{OH}}^{\text{ev}} = y_{\text{CH}_3\text{OH}} \frac{\dot{n}_{\text{dry}}}{1 - y_{\text{H}_2\text{O}} - y_{\text{CH}_3\text{OH}}} \quad (4.17)$$

$$= \frac{K_{\text{CH}_3\text{OH}} x_{\text{CH}_3\text{OH}} \dot{n}_{\text{dry}}}{1 - K_{\text{H}_2\text{O}} x_{\text{H}_2\text{O}} - K_{\text{CH}_3\text{OH}} x_{\text{CH}_3\text{OH}}} \quad (4.18)$$

$$\approx \frac{\overbrace{K_{\text{CH}_3\text{OH}}}^{f(T)}}{1 - K_{\text{H}_2\text{O}}} x_{\text{CH}_3\text{OH}} \dot{n}_{\text{dry}} \quad (4.19)$$

assuming $y_{\text{H}_2\text{O}} \approx 1$ and $y_{\text{H}_2\text{O}} \gg y_{\text{CH}_3\text{OH}}$, which is justified by the small amount of methanol compared to water in the solution.

In the *reference system*, methanol solution is in contact only with the CO_2 produced in the anodic reaction:

$$\dot{n}_{\text{dry}} = \frac{N \cdot I}{6 F} \quad (4.20)$$

In both integrated systems, the solution is in contact with the produced CO_2 and the cathode's outlet flow of incondensable gases, whose

expression is [11]:

$$\dot{n}_{\text{dry}} = \underbrace{\frac{\lambda^{\text{cath}} N}{y_{\text{O}_2, \text{dry}}^{\text{env}}}}_{\text{Entering gas flow}} \underbrace{\left(\frac{3}{2} a A \bar{c}_{\text{out}}^{\text{an}} + \frac{1-b}{4 F} I \right)}_{\text{Consumed oxygen}} \underbrace{\left(1 - \frac{y_{\text{O}_2, \text{dry}}^{\text{env}}}{3 \lambda^{\text{cath}}} \right)}_{\text{Stoichiometry}} \quad (4.21)$$

The ratio between both \dot{n}_{dry} is, by Equation 4.17, the ratio of increase in methanol loss when the *reference system*'s degasser temperature and the integrated system's separator temperature are the same.

To compensate for the increased methanol loss in the separator, which is no longer a negligible loss term as it was in the *reference system*, the feedforward concentration-control law has to be modified by adding the losses.

$$\dot{n}_{\text{CH}_3\text{OH}}^{\text{fuel}} = N \left(\frac{1-\tilde{b}}{6 F} I + \tilde{a} A \bar{c}_{\text{out}}^{\text{an}} \right) + \dot{n}_{\text{CH}_3\text{OH}}^{\text{ev}} \quad (4.22)$$

where the $\dot{n}_{\text{CH}_3\text{OH}}^{\text{ev}}$ term is calculated by means of Equations 4.19 and 4.21, and terms \tilde{a} and \tilde{b} are the feedforward controller's constant estimates of fuel cell parameters a and b , which depend on temperature.

4.2.5 Controller synthesis of highly integrated system

To increase fuel efficiency of the *highly integrated system* in comparison with the *mingled-outlet system*, it employs optimizing concentration introduced at the *two-mixer system* in Chapter 3 in order to minimize methanol loss in the separator. Air flow rate and solution volume controllers are inherited from the *reference system*, like in the case of the *mingled-outlet system* in Section 4.2.4.

4.2.5.1 Concentration controller

Methanol concentration and stack temperature are controlled by manipulating solution volume flow rate and fuel flow rate as a multi-input and multi-output (MIMO) controller. The MIMO controller is based on the concept to combine the concentration controller from *two-mixer*

system as introduced in Section 3.2.3.3 and the stack temperature controller from the *mingled-outlet system* in the previous section.

Methanol concentration is adjusted to keep the constant faradaic efficiency φ by Equation 3.2 similarly to the *two-mixer system*. However, in the *highly-integrated system*, methanol evaporation cannot be neglected because anodic outlet solution directly contacts cathodic gas products at high temperature in the separator. Therefore, methanol evaporation as in Equation 4.19 is also considered to estimate methanol loss in the *highly-integrated system*. The derivation of methanol accumulation in the separator is deduced as follows:

$$\frac{d\tilde{n}_{\text{CH}_3\text{OH}}^{\text{sep}}}{dt} = \dot{n}_{\text{CH}_3\text{OH}}^{\text{fuel}} - \left[N \left(\frac{I}{6F} (1 - \tilde{b}) + \tilde{a}A\tilde{c}_{\text{out}}^{\text{an}} \right) + \dot{n}_{\text{CH}_3\text{OH}}^{\text{ev}} \right] \quad (4.23)$$

Concentration \tilde{c}^{sep} in the integrated separator is calculated with estimated methanol amount $\tilde{n}_{\text{CH}_3\text{OH}}^{\text{sep}}$ and measured solution volume V^{sep} in the separator by Equation 3.10. The target anode inlet concentration is determined by the target faradaic efficiency φ and anode excess ratio λ^{an} with Equation 3.8.

The total methanol feed to the anode is set equal to methanol consumption by reactions and evaporation:

$$\dot{V}_{\lambda}^{\text{an}} = \frac{\lambda^{\text{an}}}{\tilde{c}_{\text{in}}^{\text{an}}} \left[N \left(\frac{I}{6F} (1 - \tilde{b}) + \tilde{a}A\tilde{c}_{\text{out}}^{\text{an}} \right) + \dot{n}_{\text{CH}_3\text{OH}}^{\text{ev}} \right] \quad (4.24)$$

When the set concentration $\tilde{c}_{\text{in}}^{\text{an}}$ is lower than the estimated concentration \tilde{c}^{sep} , fuel flow rate is set to zero to quickly reduce the concentration in the anodic loop; otherwise both methanol and solution flow rates are determined by species mass balance:

$$\begin{cases} \tilde{c}_{\text{in}}^{\text{an}} (\dot{V}^{\text{fuel}} + \dot{V}^{\text{sol}}) = \frac{\rho_{\text{CH}_3\text{OH}}}{M_{\text{CH}_3\text{OH}}} \dot{V}^{\text{fuel}} + \tilde{c}^{\text{sep}} \dot{V}^{\text{sol}} & \text{if } \tilde{c}^{\text{sep}} < \tilde{c}_{\text{in}}^{\text{an}} \\ \dot{V}^{\text{fuel}} = 0 & \text{otherwise} \end{cases} \quad (4.25)$$

4.2.5.2 Temperature controller

Another manipulated variable, solution volume flow \dot{V}_{PI}^{an} , controls stack temperature with proportional-integral (PI) controller in Equation 4.13 which is the same as that of *mingled-outlet system*. The proportional gain K_c and integral time constant τ_I are also obtained from Equations 4.11 and 4.12.

The two values \dot{V}_{λ}^{an} and \dot{V}_{PI}^{an} will in general be different; the former is set to avoid reactant starvation, and the latter regulates stack temperature. Since reactant starvation is a much faster and more critical condition than temperature deviations, the former is given priority and set as an absolute minimum for the actual value of \dot{V}^{sol} . The resulting equation is therefore:

$$\dot{V}^{an} = \dot{V}^{fuel} + \dot{V}^{sol} = \max(\dot{V}_{\lambda}^{an}, \dot{V}_{PI}^{an}) \quad (4.26)$$

4.2.5.3 Water recovery

To provide enough water to dilute neat methanol down to the set concentration, a sufficient amount of diluted solution should be maintained in the integrated separator. Liquid is recovered from water condensation in the cooler, whose temperature is set with a gain-scheduled P controller previously developed for the *reference system* in Chapter 2.1.6.2.

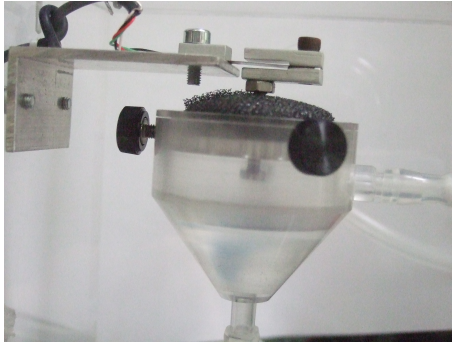


Fig. 4.3: Integrated separator in the *highly integrated system*

4.3 Experiment

Simulation of the *mingled-outlet* and *highly integrated system* is validated by experiments using the same control algorithm as in Sections 4.2.4 and 4.2.5.

4.3.1 Experimental Setup

The condenser and the cathodic cooler of the *reference system* in Chapter 2 are removed in the *mingled-outlet system* as seen in Fig. 4.1. Furthermore, the system is placed in a climate chamber (PL-3KPH, ES-PEC, Japan). The anodic cooler (Fig. 2.6b) and the degasser (Fig. 2.6c) function as loop cooler and separator respectively.

In the *highly-integrated system*, the integrated separator is designed in-house (Fig. 4.3): it separates liquid from gas and weighs the solution hold-up with a strain gauge (FSH01483, Futek, Germany). A porous medium with more than 80% of porosity covers the top of the separator to avoid liquid splash. An in-line static mixer (Plastic Mixer 103201, ESSKA.de GmbH, Germany) blends methanol solution and neat methanol in a tube before the anode inlet, similarly to the *two-mixer system* as shown in Fig. 3.1. The error range of the experiments is same as given in the error analysis in Chapter 2 because the measurement devices are identical to those of the *reference system*.

4.3.2 Operating conditions

The preconditioning of system temperature and concentration in the anodic loop to steady state is similar to that of the *reference system*: the initial temperature of the system is set to 50 °C; the climate chamber fixes the temperature at 37 °C and retains it for over 30 minutes until each system component reaches uniform temperature. During preheating, concentration is set to 1 M in the separator, and current to 1 A to activate the stack. After this initial setting, electric current is drawn according to the reference profile shown in Fig.2.10 for three hours.

4.4 Results and discussions

4.4.1 Mingled outlet system validation

The *mingled-outlet system* is operated experimentally to validate and compare both the previous model and the newly proposed one with material hold-up in the stack. The dynamic behaviour of stack temperature, methanol concentration in the anodic loop and solution weight in the mixer is compared for the different models. The voltage profiles of the stacks in the experiment and the simulations are similar to each other, as shown in Fig. 4.4.

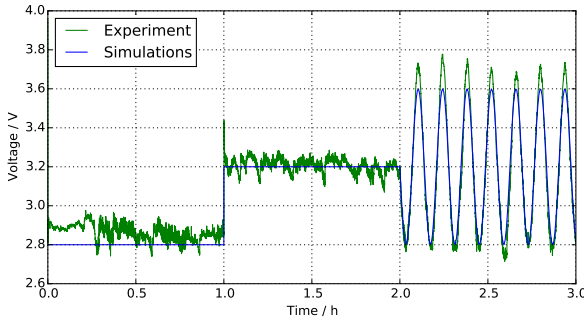


Fig. 4.4: Voltage response of the DMFC stack to the aforementioned current input for three hours in the *mingled-outlet system*

As shown in Fig. 4.5, stack temperature starts at 50 °C and rises up to 60 °C in 15 minutes. After 15 minutes, all the temperatures remain steady until the end of the operation. The temperature control algorithm works successfully for all simulations. The small temperature offset between experiment and simulation is attributed to experimentally higher methanol concentration in the anodic loop, as seen in Fig. 4.6.

After stack temperature exceeds the set temperature, the controller switches to use \dot{V}_{PT}^{an} instead of \dot{V}_{λ}^{an} at 15 minutes (Fig. 4.7). The change of active control law for flow results in a concentration peak as shown in Fig. 4.6. This switching has a negligible effect on temperature and

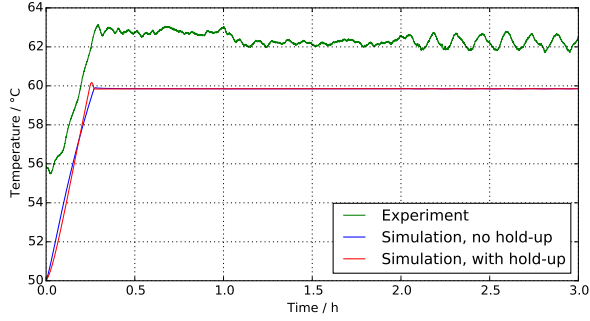


Fig. 4.5: Stack temperature profiles of the *mingled-outlet system* at the given conditions

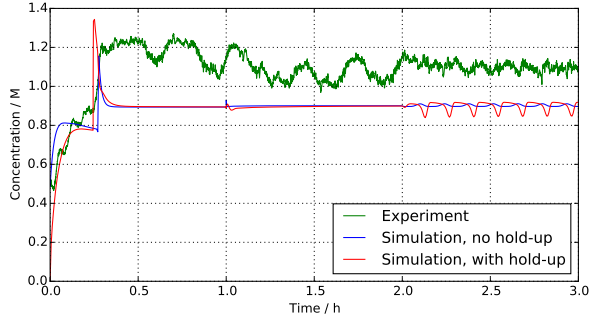


Fig. 4.6: Concentration profiles at the outlet of the separator in the *mingled-outlet system* at the given conditions

its dynamics. The mixer solution volume behaves very differently because of the liquid hold-up in the anode channel, as shown in Fig. 4.8. The larger solution volume at the beginning dampens the dynamics of mixer methanol concentration, which mitigates the slope of concentration increase (Fig. 4.6). The concentration peak of the proposed model

is higher than the other's because the solution volume in the mixer at that time is lowest. After the peak, the outlet concentration of the proposed model stabilizes slightly below 1 M.

In the experiment, concentration settles at a higher value than in simulations because of the lower temperature in the mixer (Fig. 4.9), due to the fact that the real system is not perfectly insulated; this reduces methanol loss compared to the simulation.

For the same reason, the solution flow rate into the anodic inlet in the experiment is smaller than in the simulations. The solution flow rate of PI controller \dot{V}_{PI}^{an} is calculated by Equations 4.11 and 4.13 and K_c is proportional to the inverse of the temperature difference between stack and mixer. In the experiment, the stack temperature is higher and mixer temperature is lower than in the simulations. The larger temperature difference results in smaller K_c and \dot{V}_{PI}^{an} , which lead finally to a low flow rate in experiment, as shown in Fig. 4.7.

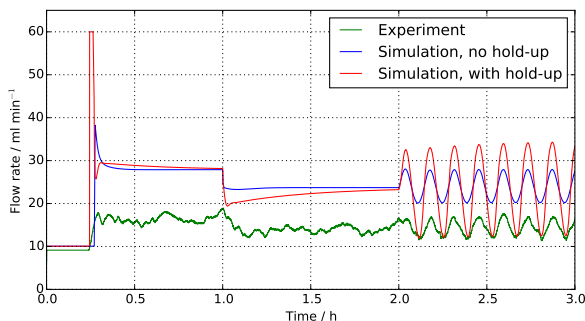


Fig. 4.7: Solution flow rate into the anode inlet of the mingled outlet stack at the given conditions

The significant difference in between the models with and without hold-up is solution accumulation. As shown in Fig. 4.8, when a high current of 3 A is drawn at the beginning, the water contained in the anodic channels of the stack flowed out to the mixer and inflated its solution volume for 15 minutes. After 15 minutes, when the solution flow rate suddenly increases as control is passed from \dot{V}_{λ}^{an} to \dot{V}_{PI}^{an} , liquid solution in the mixer almost depletes because of material hold-up in the

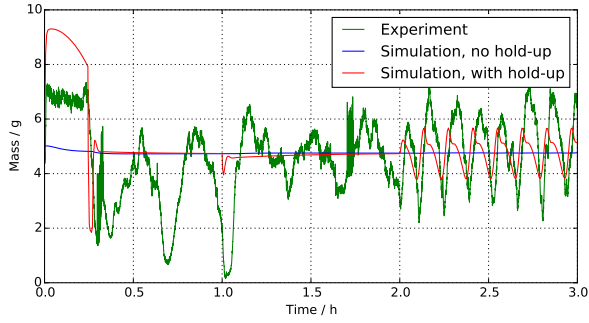


Fig. 4.8: Solution weight profiles at the mixer in the *mingled-outlet system* at the given conditions

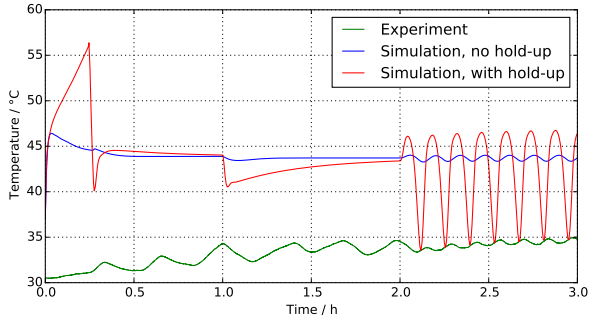


Fig. 4.9: Mixer temperature profiles of the *mingled-outlet system* at the given conditions

anode channel.

Solution volume V^{mix} fluctuates vigorously in the experiment because it is directly influenced by solution flow rate \dot{V}^{an} ; when the latter is used to control stack temperature, \dot{V}_{PI}^{an} fluctuates as an effect of feedback control.

Comparing the two simulations, the amount of solution in the mixer

hardly changes when subject to sinusoidal current in the previous model; the experiment and the new model shows high-amplitude sinusoidal responses. The oscillations in volume are caused by the increased production of carbon dioxide in the anode at higher currents, which rapidly displaces liquid to the mixer: the new model is able to capture this experimentally observed effect.

4.4.2 Highly integrated system

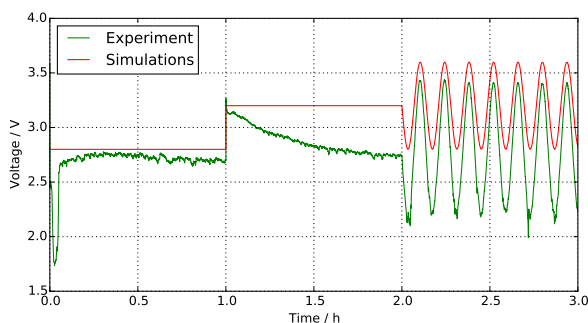


Fig. 4.10: Voltage response of the stack to the current input in the *highly-integrated system*

As in previous models, the voltage profile of the model is calculated by a Thévenin's equivalent circuit, independent from the operating temperature of the stack and methanol concentration, and this is not meant to produce an accurate prediction of voltage. Fig. 4.10 shows that experimental results feature lower voltage than the simulation, which is explained by the lower stack temperature that is obtained in the experiment: at low currents, insufficient heat is generated to maintain the desired stack temperature, as visible Fig. 4.11. Optimized control of methanol concentration in the *highly-integrated system* results in less methanol crossover for higher fuel efficiency than in the *mingled-outlet system*. In a commercial, compact system, the low stack temperature is not likely to be an issue, since the tightly integrated and insulated component will maintain heat better than the laboratory setup.

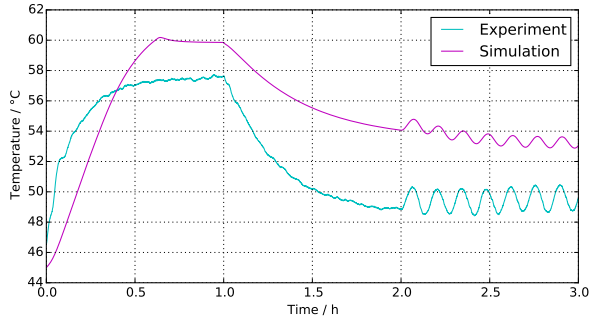


Fig. 4.11: Stack temperature profiles of the *highly-integrated system* at the given conditions

In the experiment, concentration is measured after separation because the sensor cannot operate on a two phase flow: the measurement is therefore lower than the actual anode outlet concentration because of methanol evaporation in the separator. During start-up, concentration reaches a minimum after a few seconds (Fig. 4.12), which is caused by the fast load change from 1 A to 3 A. The sudden current increase causes methanol starvation at the catalyst layer until highly concentrated solution can compensate for it. After an hour, the concentration profile from the experimental result is higher than that of the simulation because of overestimated methanol crossover. While the control parameters for the estimation of methanol crossover \tilde{a} and \tilde{b} are calibrated at 60 °C, the actual crossover is reduced by the lower temperature of the stack (see Fig. 4.11).

The solution buffer in the experiment is not located only in the stack and mixer as simulations: the liquid in tubes and the cooler mitigates rapid concentration changes. Therefore, the concentration profile in the experiment is not as steep as in the simulation, but shows a smooth curve after the current step after 1 hour.

The initial peak of solution weight (see Fig. 4.13) results from liquid hold up: when the current steps up from 1 A to 3 A just after start-up, the produced carbon dioxide gas immediately pushes out liquid from the stack, raising the solution weight from 5 g to 10 g in a short

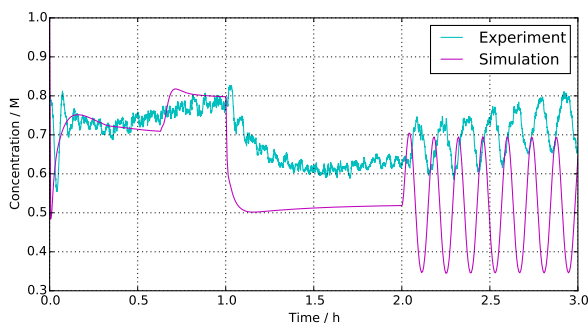


Fig. 4.12: Concentration profiles at the outlet of the separator in the *highly-integrated system* at the given conditions

time. After reaching the set value after about one hour, the solution weight profile in the simulation converges to the steady state, whereas the one from the experimental results oscillates within an amplitude of about 2g because of the two phase volume change in the cooler. Shrinking gas volume after cooling slowed down solution flow rate to the integrated separator. This volume change of gas in the cooler did not affect solution volume in the other systems because buffers such as a separator, a degasser or a condenser mitigate sudden changes. If the cooler is modelled with material hold up for two phase mixture, it may be able to simulate volume contraction of gas precisely in the future. In a real system, a heat exchanger with high heat exchanging efficiency or small heat mass can reduce the solution weight fluctuation.

4.4.3 Efficiency

In the experiment, the fuel tank was weighed by the electric scale to calculate methanol consumption. The discontinuous pumping of the peristaltic pump disturbs the sensitive balance, producing noise as visible in Fig. 4.14. However, both simulation and experimental fuel efficiencies match well. Over the whole period, the *highly-integrated system* has higher fuel efficiency than the *mingled-outlet system* due to optimized concentration control (Fig. 4.12), which leads to less methanol loss.

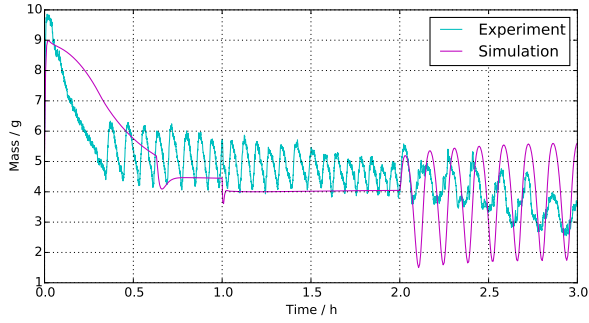


Fig. 4.13: Solution weight profiles at the tank buffer in the *highly-integrated system* at the given conditions

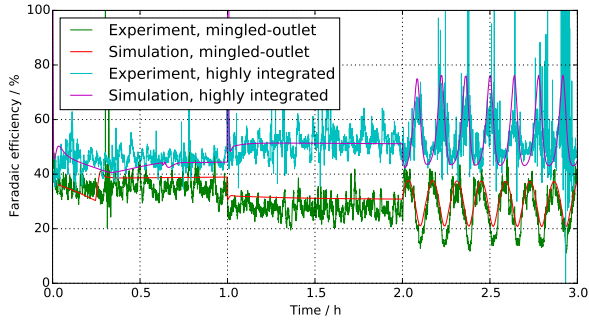


Fig. 4.14: Fuel efficiencies of the *mingled-outlet system* and the *highly-integrated system* at the given conditions

The overall efficiency profile is slightly different from the fuel efficiency, as shown in Fig. 4.15. During the whole period, the *highly-integrated system* is more efficient than the *mingled-outlet system* because of the optimal concentration control especially at the lower current. The small gap between the model and experiment in the *highly-*

integrated system at the current 2 A (from one hour to two hours) results from the lower voltage at the lower temperature in experiment.

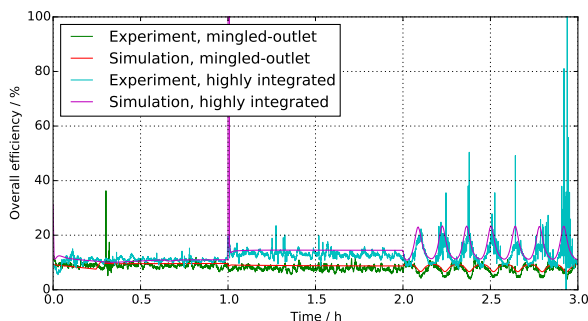


Fig. 4.15: Overall efficiencies of the *mingled-outlet system* and the *highly-integrated system* at the given conditions

4.5 Conclusions

In the previous research, the *mingled-outlet system* was suggested as a simplification of the *reference system*, which however had lower efficiency due to high methanol evaporation in the separator: this also constrains the use of portable DMFC systems to outdoor applications for health reasons.

In this chapter, the simulation of the *mingled-outlet system* model has been validated, and experiments are executed with the same parameters and controllers as in the simulations. In the experiments, the solution volume is not only accumulated in the mixer, but also in the stack's anode channels, in tubing and other units. The stack model, modified with material hold-up in the anode channel, was able to reproduce experimentally observed dynamic behaviour of the solution weight better than the previous model. Therefore, the relatively big channel volume of the stack should be simulated with material hold up.

The *highly-integrated system* is proposed for higher efficiency and fewer components than the *mingled-outlet system*, integrating the mixer

and the separator. The compact design of the *highly-integrated system* is appropriate for portable applications such as laptops or leisure power sources, though in general the overall efficiency is relatively small. Despite compactness and higher efficiency, the *highly-integrated system* still has disadvantages due to huge methanol evaporation and low tolerance to rapid current increases, which can cause temporary methanol starvation. When dynamic load following up is necessary, the load ramp-up should be moderated to prevent the starvation, possibly by hybridisation with buffer batteries. If it runs within the stable range of the operation, the *highly-integrated system* will be useful and efficient to supply electricity to the off-grid power units.

Chapter 5

Summary and outlook

DMFC systems as portable power sources are required to be compact and light. To achieve these requirements, various advanced designs of DMFC systems are introduced and analysed systematically with model simulation and experimental validation. The *reference system* is defined for each system component to have its own function and to prove feasibility of autonomous operation. The other systems optimized components to enhance efficiency or integrated processes to reduce the number of system components.

Firstly, the *reference system* model is validated experimentally at steady state. The simulation of consumed methanol with crossover and evaporation of the model is quantitatively matching to those of experiments. The feasibility envelope for operating a system autonomously with stable water level is compared with the experiments at different temperatures and relative humidities. With this validation, it is found that the *reference system* model is successfully verified at atmospheric temperature conditions. Dynamic behaviour was also successfully validated with the same controllers of the system model.

Secondly, two modified systems from the *reference system* are proposed to increase efficiency. One is the *two-mixer system* with in-line static mixer between the tank mixer and the stack. It showed higher efficiency than the *reference system* and the *separate-tank system*, which, though, has additional components comparing to the other systems. The *separate-tank system* is equipped with two tanks and pumps for water and methanol solution, respectively. Dynamic concentration control with differently concentrated solutions results in less methanol loss and higher efficiency than constant concentration control in the *reference system*. These highly efficient systems enable to extend operating time or reduce fuel tank size for portable applications. In both modified systems, the dynamic concentration control algorithm is implemented

Table 5.1: Summary of qualitative evaluation of DMFC systems

	Compactness	Faradaic efficiency	Overall efficiency
Reference system	o	o	↓
Two-mixer system	o	↑	↑
Separate-tank system	↓	↑	↑
Mingled-outlet system	↑	↓	↓
Highly-integrated system	↑	o	o

and successfully validated with experiments.

Thirdly, to reduce the number of components and system size, anode and cathode outlets are combined and the two separators and two coolers are reduced to one each. The influences of the process integration are analysed, and pros and cons are investigated. The main advantage of the integration is that the resulting system is compact and light. However, large amount of methanol evaporates after direct contact with hot air from cathode outlet. This causes a low fuel efficiency for the integrated system. To proceed further in integration, a *highly-integrated system* is developed with the combination of the separator and the mixer. Despite the smaller size, the efficiency is better than the *mingled-outlet system* because the dynamic concentration control algorithm reduces methanol evaporation. Due to the high fuel efficiency with small size system, the *highly-integrated system* is superior to the *reference system*. Additionally the more realistic model with material hold up in the anodic channel of the stack, is able to simulate the dynamic behaviour of water recovery closer to actual systems than the previous model. However, at several cases, two phase flow disturbed controllers such as solution volume or concentration control.

Each system is qualitatively compared with three different point of views in Table 5.1. The *two-mixer system* has higher efficiencies than the reference system with similar compactness and simpler than the *separate-tank system*. The size of the *highly-integrated system* is smallest among the systems even though it has higher performance than the *reference system*. I hope that using the relative comparison, fuel cell engineers can choose the more suitable system for their specific applications.

In the future, if the material hold up is considered at other components as well, models would be able to simulate each system even with high precision. Finally, tightly integrated components in a compact and well-insulated system can give more practical information to design direct methanol fuel cell systems.

Nomenclature

5.1 Latin symbols

a	Crossover parameter [= $1.6748 \times 10^{-6} \text{m/s}$]
A	Active area [= 0.003m^2]
b	Crossover parameter [=0.173]
c	Methanol concentration [mol/m^3]
C_p	Heat capacity [J/K]
c_p	Heat capacity by volume [$\text{J/m}^3 \text{K}$]
d	Membrane thickness [m]
D	Diffusion coefficient of methanol [m^2/s]
e	Error of temperature [$^{\circ}\text{C}$]
E	Internal energy [J]
i	Current density [A/cm^2]
I	Current [A]
F	Faraday constant [=96 485 C/mol]
f	Function of vapour mole fraction [–]
Δg_r	Reaction Gibbs free energy [= -702kJ/mol]
h	Molar enthalpy [J/mol]
Δh_r	Reaction Enthalpy [= -726kJ/mol]
K	Equilibrium constant [–]
K_c	P constant in PI controller [$\text{m}^3/\text{s K}$]
k_d	Electro-osmotic drag coefficient [–]
k_m	Mass transfer coefficient [–]
M	Molar mass [kg/mol]
N	Number of cells [=9]
n	Amount of substance [mol]
p	Pressure [Pa]
R	Resistance [= 0.4Ω]
s	Laplace variable [s^{-1}]
T	Temperature [K]
t	Time [s]
U	Voltage [V]

U_0	Open-circuit voltage [V]
V	Volume [m^3]
W	Weight [g]
x	Molar fraction in liquid phase [–]
y	Molar fraction in gas phase [–]
z	Overall molar fraction [–]

5.2 Greek symbols

β	Vapour molar fraction [–]
γ	Activity coefficient [–]
η	Overall efficiency [–]
φ	Faradaic efficiency [–]
ε	Electrochemical efficiency [–]
λ	Excess ratio [–]
ν	Current stoichiometric coefficient [–]
π	Vapour pressure [Pa]
ξ	Crossover stoichiometric coefficient [–]
ρ	Density [kg/m^3]
σ	Conditional-integration flag [–]
τ	Time constant [s]

5.3 Superscripts

air	Air
an	Anode
cath	Cathode
comp	Components (CH_3OH , H_2O , N_2 , O_2 , CO_2)
cond	Condenser
deg	Degasser
env	Environment
ev	Evaporation
fuel	Fuel
gas	Gas
holdup	Holdup
int	Integrated
liq	Liquid
CH_3OH	Methanol

mix	Mixer
ref	Reference
sat	Saturation
sep	Separator
s	Side of anode or cathode
sol	Solution, or solution tank
stack	Stack
water	Water

5.4 Subscripts

c	Concentration
cl	Catalyst layer
d	Electro-osmotic drag
dry	Incondensable gases (N_2 , O_2 , CO_2)
flows	Flows to the mixer from condenser, degasser or fuel reservoir
in	Inlet
j	Species
o	Initial value
out	Outlet
V	Volume
x	Crossover

5.5 Diacritics

\tilde{o}	Estimate
\bar{o}	Set point
\dot{o}	Flow [s^{-1}]
\check{o}	Minimum
\hat{o}	Maximum

Bibliography

- [1] Federico Zenith and Ulrike Krewer. Modelling, dynamics and control of a portable DMFC system. *Journal of Process Control*, 20(5):630–642, 2010.
- [2] Dan Carter, Marge Ryan, and Jonathan Wing. Fuel cell industry review 2012. Technical report, Fuel Cell Today, 2012. URL <http://www.fuelcelltoday.com/analysis/industry-review>.
- [3] Omar Z Sharaf and Mehmet F Orhan. An overview of fuel cell technology: Fundamentals and applications. *Renewable and Sustainable Energy Reviews*, 32:810–853, 2014.
- [4] Han-Ik Joh, Tae Jung Ha, Sang Youp Hwang, Jong-Ho Kim, Seung-Hoon Chae, Jae Hyung Cho, Joghee Prabhuram, Soo-Kil Kim, Tae-Hoon Lim, Baek-Kyu Cho, et al. A direct methanol fuel cell system to power a humanoid robot. *Journal of Power Sources*, 195(1):293–298, 2010.
- [5] Tony Thampan, Dinesh O Shah, C Cook, J Novoa, and Sunil N Shah. Development and evaluation of portable and wearable fuel cells for soldier use. *Journal of Power Sources*, 259:276–281, 2014.
- [6] Kai Sundmacher and Keith Scott. Direct methanol polymer electrolyte fuel cell: analysis of charge and mass transfer in the vapour–liquid–solid system. *Chemical Engineering Science*, 54(13):2927–2936, 1999.
- [7] Siti Kartom Kamarudin, Wan Ramli Wan Daud, Sze Ling Ho, and Umi Azmah Hasran. Overview on the challenges and developments of micro-direct methanol fuel cells (DMFC). *Journal of Power Sources*, 163(2):743–754, 2007.
- [8] Jean Marie Tarascon and Michel Armand. Issues and challenges facing rechargeable lithium batteries. *Nature*, 414(6861):359–367, 2001.

- [9] Robert H Perry, Donald W Green, and James O Maloney. *Perry's chemical Engineers' handbook 7th ed.* McGraw-Hill, USA, 1997.
- [10] Jun-Young Park, Ka-Young Park, Ki Buem Kim, Youngseung Na, Hyejung Cho, and Joon-Hee Kim. Influence and mitigation methods of reaction intermediates on cell performance in direct methanol fuel cell system. *Journal of Power Sources*, 196(13): 5446–5452, 2011.
- [11] Federico Zenith, Christine Weinzierl, and Ulrike Krewer. Model-based analysis of the feasibility envelope for autonomous operation of a portable direct methanol fuel-cell system. *Chemical Engineering Science*, 65(15):4411–4419, 2010.
- [12] Tae Jung Ha, Jong-Ho Kim, Han-Ik Joh, Soo-Kil Kim, Go-Young Moon, Tae-Hoon Lim, Chonghun Han, and Heung Yong Ha. Sensor-less control of methanol concentration based on estimation of methanol consumption rates for direct methanol fuel cell systems. *International Journal of Hydrogen Energy*, 33(23):7163–7171, 2008.
- [13] Joon-Hee Kim, Min-Jee Yang, and Jun-Young Park. Improvement on performance and efficiency of direct methanol fuel cells using hydrocarbon-based membrane electrode assembly. *Applied Energy*, 115:95–102, 2014.
- [14] Ming-Chi Tsai, Tsung-Kuang Yeh, Charn-Ying Chen, and Chuen-Horng Tsai. A catalytic gas diffusion layer for improving the efficiency of a direct methanol fuel cell. *Electrochemistry Communications*, 9(9):2299–2303, 2007.
- [15] Jeremy P Meyers and Brent Bennett. Analytical model to relate dmfc material properties to optimum fuel efficiency and system size. *Journal of Power Sources*, 196(22):9473–9480, 2011.
- [16] Jun-Young Park, Yongho Seo, Sangkyun Kang, Daejong You, Hyejung Cho, and Youngseung Na. Operational characteristics of the direct methanol fuel cell stack on fuel and energy efficiency with performance and stability. *International Journal of Hydrogen Energy*, 37(7):5946–5957, 2012.

- [17] Kyungmun Kang, Giyong Lee, Geonhui Gwak, Yongjun Choi, and Hunchul Ju. Development of an advanced mea to use high-concentration methanol fuel in a direct methanol fuel cell system. *International Journal of Hydrogen Energy*, 37(7):6285–6291, 2012.
- [18] Stefanie v Andrian and Josefin Meusinger. Process analysis of a liquid-feed direct methanol fuel cell system. *Journal of Power Sources*, 91(2):193–201, 2000.
- [19] Stefania Specchia, Ugo A Icardi, Vito Specchia, and Guido Saracco. Compact direct methanol fuel cells for portable applications: a modeling study. *International Journal of Chemical Reactor Engineering*, 3(1), 2005.
- [20] Alexander Mitsos, Benoît Chachuat, and Paul I Barton. What is the design objective for portable power generation: Efficiency or energy density? *Journal of power sources*, 164(2):678–687, 2007.
- [21] Hendrik Dohle, Jürgen Mergel, and Detlef Stolten. Heat and power management of a direct-methanol-fuel-cell (dmfc) system. *Journal of Power Sources*, 111(2):268–282, 2002.
- [22] Christopher K Dyer. Fuel cells for portable applications. *Journal of Power Sources*, 106(1):31–34, 2002.
- [23] HaeKyoung Kim. Passive direct methanol fuel cells fed with methanol vapor. *Journal of power sources*, 162(2):1232–1235, 2006.
- [24] Weimin Qian, David P Wilkinson, Jun Shen, Haijiang Wang, and Jiujuun Zhang. Architecture for portable direct liquid fuel cells. *Journal of power sources*, 154(1):202–213, 2006.
- [25] Jianyu Cao, Zhiqing Zou, Qinghong Huang, Ting Yuan, Zhilin Li, Baojia Xia, and Hui Yang. Planar air-breathing micro-direct methanol fuel cell stacks based on micro-electronic-mechanical-system technology. *Journal of Power Sources*, 185(1):433–438, 2008.
- [26] Yuming Yang and Yung C Liang. A direct methanol fuel cell system with passive fuel delivery based on liquid surface tension. *Journal of power sources*, 165(1):185–195, 2007.

- [27] Federico Zenith and Ulrike Krewer. Simple and reliable model for estimation of methanol cross-over in direct methanol fuel cells and its application on methanol-concentration control. *Energy & Environmental Science*, 4(2):519–527, 2011.
- [28] Youngseung Na, Federico Zenith, and Ulrike Krewer. Increasing fuel efficiency of direct methanol fuel cell systems with feedforward control of the operating concentration. *Energies*, 8(9):10409–10429, 2015.
- [29] Curtis H Whitson and Michael L Michelsen. The negative flash. *Fluid Phase Equilibria*, 53:51–71, 1989.
- [30] Thorsten Schultz. *Experimental and model-based analysis of the steady-state and dynamic operating behaviour of the direct methanol fuel cell (DMFC)*. PhD thesis, Otto-von-Guericke-Universität Magdeburg, 2004.
- [31] Ryan O'Hare, Suk-Won Cha, WG Colella, and FB Prinz. *Fuel cell fundamentals*. Wiley, Hoboken, NJ, 2009.
- [32] Keith Scott, WM Taama, Sven Kramer, Panos Argyropoulos, and Kai Sundmacher. Limiting current behaviour of the direct methanol fuel cell. *Electrochimica Acta*, 45(6):945–957, 1999.
- [33] Thomas Schaffer, Thomas Tschinder, Viktor Hacker, and Jürgen O Besenhard. Determination of methanol diffusion and electroosmotic drag coefficients in proton-exchange-membranes for dmfc. *Journal of power sources*, 153(2):210–216, 2006.
- [34] Xiaoming Ren and Shimshon Gottesfeld. Electro-osmotic drag of water in poly (perfluorosulfonic acid) membranes. *Journal of The Electrochemical Society*, 148(1):A87–A93, 2001.
- [35] Eric W Lemmon, Mark O McLinden, and Daniel G Friend. NIST chemistry webbook, thermophysical properties of fluid systems, NIST standard reference database number 69. <http://webbook.nist.gov>, 2011. Accessed: 2015-07-01.
- [36] Sigurd Skogestad. Simple analytic rules for model reduction and PID controller tuning. *Journal of Process Control*, 13(4):291–309, 2003.

- [37] Federico Zenith, Youngseung Na, and Ulrike Krewer. Effects of process integration in an active direct methanol fuel-cell system. *Chemical Engineering and Processing: Process Intensification*, 59: 43–51, 2012.
- [38] Srikanth Arisetty, Cedric A Jacob, Ajay K Prasad, and Suresh G Advani. Regulating methanol feed concentration in direct methanol fuel cells using feedback from voltage measurements. *Journal of Power Sources*, 187(2):415–421, 2009.
- [39] Younghyun Kim, Donghwa Shin, Jueun Seo, Naehyuck Chang, Hyejung Cho, Youngjae Kim, and Seongkee Yoon. System integration of a portable direct methanol fuel cell and a battery hybrid. *International Journal of Hydrogen Energy*, 35(11):5621–5637, 2010.
- [40] Youngseung Na, Jungmin Kwon, Hyun Kim, Hyejung Cho, and Inseob Song. Characteristics of a direct methanol fuel cell system with the time shared fuel supplying approach. *Energy*, 50:406–411, 2013.

List of Tables

2.1	The stoichiometric coefficients for main reaction ν_j^s and crossover ξ_j^s for each species on cathode and anode. . . .	26
2.2	Summary of the proposed controllers for the reference DMFC system	29
2.3	Operating conditions for steady state analysis of the DMFC system	38
3.1	Model equations and parameters valid for <i>reference, two-mixer and separate-tank system</i> models	55
3.2	Identical controllers for <i>reference, two-mixer and separate-tank systems</i>	56
3.3	Absolute root mean square error between experiment and simulation of each system for stack temperature, inlet and outlet concentration	63
5.1	Summary of qualitative evaluation of DMFC systems . .	98

List of Figures

1.1	Schematic diagram of direct methanol fuel cell	16
1.2	Exemplary schematic diagram of (a) an open loop system and (b) closed system for DMFCs	18
2.1	The process layout of the <i>reference system</i> [1].	22
2.2	The block diagram of gas-liquid separator in fuel cell systems	27
2.3	The block diagram of mixer in the <i>reference system</i> of direct methanol fuel cells	28
2.4	The block diagram of P controller for water recovery in the condenser	31
2.5	The <i>reference system</i> of the direct methanol fuel cell in the climate chamber	33
2.6	Taylor made components in the direct methanol fuel cell system	35
2.7	T-shape casing of a thermocouple probe for measuring gas temperature	36
2.8	(a) The sketch of the weighing mechanism of a tank with the strain gauge and (b) the picture of the actual mixer attached to the strain gauge.	37
2.9	Grid map for setting temperature and relative humidity in the climate chamber	38
2.10	Input current to all DMFC systems with 9 cells and 30 cm ² as an active area	39
2.11	Water accumulation during constant current operation of the <i>reference system</i> at different relative humidity of 20% (a) and 90% (b) at a temperature of 57°C	42
2.12	Water accumulation during constant current operation of the <i>reference system</i> at (a) condition 1 and (b) condition 2 in Table 2.3 and plate at 0 to denote stable water level	46

2.13	Feasibility envelopes for the autonomous operation of the <i>reference system</i> at condition 1 with those (a) at condition 2, (b) at condition 3 or (c) at condition 4 in Table 2.3	47
2.14	The temperature profile of the stack in the <i>reference system</i>	48
2.15	Outlet concentration profile in the anodic loop of the <i>reference system</i>	48
2.16	Solution weight during operation of the mixer in the <i>reference system</i>	49
3.1	The process layout of the <i>two-mixer system</i>	52
3.2	The process layout of the <i>separate-tank system</i>	53
3.3	The block diagram of the MIMO feedforward concentration and λ controller in the <i>two-mixer system</i>	60
3.4	The block diagram of the concentration and volume controller in the <i>separate-tank system</i>	62
3.5	the resulting output voltage in simulations and experiments for all systems.	64
3.6	The temperature profile of the stack in (a) <i>two-mixer system</i> and (b) <i>separate-tank system</i>	65
3.7	Stack inlet and outlet concentrations for all systems(Estimated values are calculated identically in both simulation and experiment	66
3.8	(a) Solution weight measurement of the tank mixer in the <i>two-mixer system</i> , (b) solution weight of the solution tank and (c) water weight of the water tank in the <i>separate-tank system</i> , respectively	68
3.9	Faradaic Efficiencies of the various systems in simulations and experiments.	70
4.1	The process scheme of the <i>mingled-outlet system</i> [37] . .	74
4.2	The process scheme of the <i>highly-integrated system</i> . . .	75
4.3	Integrated separator in the <i>highly integrated system</i> . . .	84
4.4	Voltage response of the DMFC stack to the aforementioned current input for three hours in the <i>mingled-outlet system</i>	86
4.5	Stack temperature profiles of the <i>mingled-outlet system</i> at the given conditions	87
4.6	Concentration profiles at the outlet of the separator in the <i>mingled-outlet system</i> at the given conditions	87

4.7	Solution flow rate into the anode inlet of the mingled outlet stack at the given conditions	88
4.8	Solution weight profiles at the mixer in the <i>mingled-outlet system</i> at the given conditions	89
4.9	Mixer temperature profiles of the <i>mingled-outlet system</i> at the given conditions	89
4.10	Voltage response of the stack to the current input in the <i>highly-integrated system</i>	90
4.11	Stack temperature profiles of the <i>highly-integrated system</i> at the given conditions	91
4.12	Concentration profiles at the outlet of the separator in the <i>highly-integrated system</i> at the given conditions . . .	92
4.13	Solution weight profiles at the tank buffer in the <i>highly-integrated system</i> at the given conditions	93
4.14	Fuel efficiencies of the <i>mingled-outlet system</i> and the <i>highly-integrated system</i> at the given conditions	93
4.15	Overall efficiencies of the <i>mingled-outlet system</i> and the <i>highly-integrated system</i> at the given conditions	94